ISSN 2096-7071
CN 10-1629/R1

CHINA CDC WEEKLY

Vol. 5 No. 5 Feb. 3, 2023

CCDC weekly

中国疾病预防控制中心周报

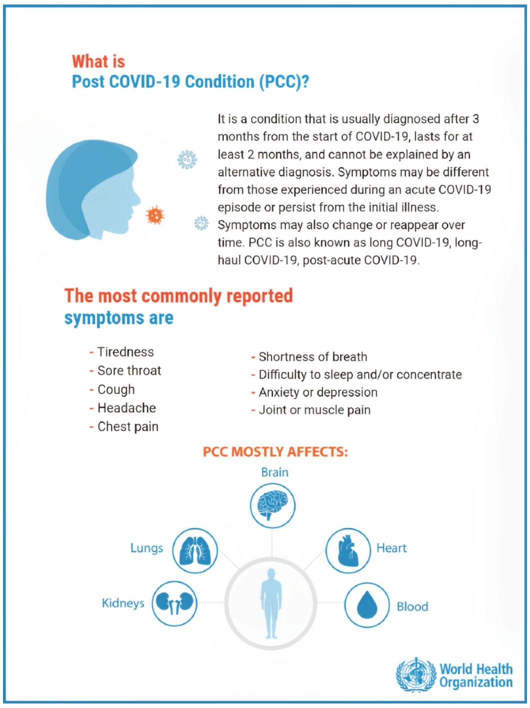

What is
Post COVID-19 Condition (PCC)?

It is a condition that is usually diagnosed after 3 months from the start of COVID-19, lasts for at least 2 months, and cannot be explained by an alternative diagnosis. Symptoms may be different from those experienced during an acute COVID-19 episode or persist from the initial illness. Symptoms may also change or reappear over time. PCC is also known as long COVID-19, long-haul COVID-19, post-acute COVID-19.

The most commonly reported symptoms are

- Tiredness
- Sore throat
- Cough
- Headache
- Chest pain
- Shortness of breath
- Difficulty to sleep and/or concentrate
- Anxiety or depression
- Joint or muscle pain

PCC MOSTLY AFFECTS:

World Health Organization

COVID-19 ISSUE (34)

Preplanned Studies

Methods and Applications

ISSN 2096-7071

Editorial Board

Editor-in-Chief Hongbing Shen
Founding Editor George F. Gao
Deputy Editor-in-Chief Liming Li Gabriel M Leung Zijian Feng
Executive Editor Feng Tan
Members of the Editorial Board
Rui Chen
Wen Chen
Xi Chen (USA)
Zhuo Chen (USA)
Gangqiang Ding
Xiaoping Dong
Pei Gao
Mengjie Han
Yuantao Hao
Na He
Yuping He
Guoqing Hu
Zhibin Hu
Yueqin Huang
Na Jia
Weihua Jia
Zhongwei Jia
Guangfu Jin
Xi Jin
Biao Kan
Haidong Kan
Ni Li
Qun Li
Ying Li
Zhenjun Li
Min Liu
Qiyong Liu
Xiangfeng Lu
Jun Lyu
Huilai Ma
Jiaqi Ma
Chen Mao
Xiaoping Miao
Ron Moolenaar (USA)
Daxin Ni
An Pan
Lance Rodewald (USA)
William W. Schluter (USA)
Yiming Shao
Xiaoming Shi
Yuelong Shu
RJ Simonds (USA)
Xuemei Su
Chengye Sun
Quanfu Sun
Xin Sun
Jinling Tang
Huaqing Wang
Hui Wang
Linhong Wang
Tong Wang
Guizhen Wu
Jing Wu
Xifeng Wu (USA)
Yongning Wu
Zunyou Wu
Min Xia
Ningshao Xia
Yankai Xia
Lin Xiao
Wenbo Xu
Hongyan Yao
Zundong Yin
Dianke Yu
Hongjie Yu
Shicheng Yu
Ben Zhang
Jun Zhang
Liubo Zhang
Wenhua Zhao
Yanlin Zhao
Xiaoying Zheng
Maigeng Zhou
Xiaonong Zhou
Guihua Zhuang

Advisory Board

Director of the Advisory Board Jiang Lu
Vice-Director of the Advisory Board Yu Wang Jianjun Liu Jun Yan
Members of the Advisory Board
Chen Fu
Gauden Galea (Malta)
Dongfeng Gu
Qing Gu
Yan Guo
Ailan Li
Jiafa Liu
Peilong Liu
Yuanli Liu
Kai Lu
Roberta Ness (USA)
Guang Ning
Minghui Ren
Chen Wang
Hua Wang
Kean Wang
Xiaoqi Wang
Zijun Wang
Fan Wu
Xianping Wu
Jingjing Xi
Jianguo Xu
Gonghuan Yang
Tilahun Yilma (USA)
Guang Zeng
Xiaopeng Zeng
Yonghui Zhang
Bin Zou

Editorial Office

Directing Editor Feng Tan
Managing Editors Lijie Zhang Yu Chen Peter Hao (USA)
Senior Scientific Editors Ning Wang Ruotao Wang Shicheng Yu Qian Zhu
Scientific Editors Weihong Chen Xudong Li Nankun Liu Liwei Shi
Liuying Tang Meng Wang Zhihui Wang Xi Xu
Qing Yue Ying Zhang

Cover Image: adapted from the World Health Organization, https://www.paho.org/en/topics/coronavirus-infections/coronavirus-disease-covid-19-pandemic/post-covid-19-condition.
This week's issue was organized by Guest Editor Hongjie Yu.

Preplanned Studies

Risk Factors Associated with the Spatiotemporal Spread of the SARS-CoV-2 Omicron BA.2 Variant — Shanghai Municipality, China, 2022

Wen Zheng[1]; Xiaowei Deng[1]; Cheng Peng[1]; Xuemei Yan[1]; Nan Zheng[1]; Zhiyuan Chen[1]; Juan Yang[1]; Marco Ajelli[2]; Juanjuan Zhang[1,#]; Hongjie Yu[1,3,#]

Summary

What is already known about this topic?

Previous studies have explored the spatial transmission patterns of severe acute respiratory syndrome coronavirus 2 (SARS-CoV-2) and have assessed the associated risk factors. However, none of these studies have quantitatively described the spatiotemporal transmission patterns and risk factors for Omicron BA.2 at the micro (within-city) scale.

What is added by this report?

This study highlights the heterogeneous spread of the 2022 Omicron BA.2 epidemic in Shanghai, and identifies associations between different metrics of spatial spread at the subdistrict level and demographic and socioeconomic characteristics of the population, human mobility patterns, and adopted interventions.

What are the implications for public health practice?

Disentangling different risk factors might contribute to a deeper understanding of the transmission dynamics and ecology of coronavirus disease 2019 and an effective design of monitoring and management strategies.

An Omicron BA.2 epidemic occurred in Shanghai, China in early March 2022. The objective of our study is to quantify the spatial spread of the epidemic across Shanghai subdistricts and identify risk factors. This study provides quantitative estimates of the epidemic arrival time, growth rate, and infection attack rate (IAR) as of May 31, 2022, and uses a generalized linear mixed effect model (GLMM) to explore their associations with demographic and socioeconomic characteristics of the population, human mobility, and interventions at the subdistrict level. We found that the epidemic growth rate was positively associated with the epidemic arrival time and subdistricts farther away from the (likely) origin of the outbreak had lower growth rates. The IAR was negatively correlated with the arrival time, distance from the initial outbreak location, subdistrict location, and booster coverage in the population aged 65 years and above; a positive association was found for population density and gross domestic product (GDP). This study highlights the role of the geographical structure of the city, human mobility, population characteristics, and adopted interventions in shaping the dynamics of the epidemic.

Shanghai is divided into 16 districts and 216 subdistricts. In the initial phase of the outbreak, grid management was implemented at the subdistrict level and entailed partial lockdown and mass nucleic acid screening for high-risk areas and non-high-risk areas. Afterward, eastern Shanghai entered a population-wide lockdown on March 28, and then the rest of Shanghai entered a lockdown phase on April 1 (Supplementary Figure S1, available in https://weekly.chinacdc.cn/). The city-wide lockdown was fully lifted on June 1, 2022.

Daily aggregated data on the number of infections and individual-level data of all severe acute respiratory syndrome coronavirus 2 (SARS-CoV-2) infections were extracted from multiple publicly available official data sources. The initial (identified) focus of the outbreak was the cultural activity center of Shiquan subdistrict in Putuo District, where a cluster of 14 SARS-CoV-2 positive individuals was detected starting from March 1, 2022 (*1*).

To describe the time course of the Omicron outbreak in Shanghai, we estimated the following three indicators at the subdistrict level: 1) epidemic arrival time (i.e., the date of the first confirmed infection in a subdistrict), 2) IAR (i.e., the cumulative number of reported infections in a subdistrict divided by the total population in that subdistrict), and 3) epidemic growth rate.

To explore potential risk factors associated with the epidemic arrival time, growth rate, and IAR across subdistricts, we included several covariates that belong to four general categories: demographic characteristics, socioeconomic characteristics, human mobility, and interventions (Supplementary Table S1, available in https://weekly.chinacdc.cn/). The arrival time of the epidemic represents a response variable when measuring the spread of the infection; however, we also considered it as an explanatory variable when exploring its association with the epidemic growth rate and IAR.

A correlation analysis was conducted to assess collinearities between the independent variables. We built a GLMM model to estimate the proportion of variance in the response variables ascribable to intra- and inter-district variation. The significance level was set to 0.1 for candidate variable selection, and 0.05 for multivariate regression. To test whether the random model was appropriately chosen, we also estimated spatial autocorrelation between residuals using Moran's *I* statistic. To quantify the uncertainty of model selection, a generalized estimating equation (GEE) model accounting for spatial clustering was used in a sensitivity analysis. The detailed statistical methods are presented in the Supplementary Material. All the analyses were performed in R 4.1.0 (R Foundation for Statistical Computing, Vienna, Austria).

As of May 31, 2022, a total of 626,840 SARS-CoV-2 infections had been reported in 99.54% of the Shanghai subdistricts. High heterogeneity in the spatial distribution of infections was found across subdistricts, with 27.78% of the subdistricts accounting for more than 70% of all infections (Supplementary Figure S2, available in https://weekly.chinacdc.cn/).

The spatial spread of the epidemic showed a clear spatial trend from the city center to adjacent areas, and a continuous spread toward suburban and rural areas. The spatial distribution of the arrival time was highly heterogeneous, with 35.19%, 41.67%, and 97.69% of the subdistricts reporting infections within the first week, second week, and a month, respectively.

We analyzed the correlation between the epidemic arrival time and the geographical distance from the initial outbreak location. The regression model showed that compared to the geographic and effective distances, the pre-epidemic flow of travelers showed a slightly weaker correlation with the epidemic arrival time (Figure 1).

By fitting a linear regression model to the logarithm of the daily number of new confirmed infections from February 26 to April 1, 2022, the overall epidemic growth rate for Shanghai was estimated to be 0.23 per day [95% confidence interval (*CI*): 0.22–0.25]. Excluding 6 subdistricts reporting no infections before the lockdown and 49 subdistricts with R^2<0.6, as well as 3 subdistricts with only two data points, we analyzed the estimated growth rates for the remaining 158 subdistricts. The growth rate was lognormal-distributed, with a range of 0.06 to 0.39, which was positively associated with the arrival time of the epidemic (Figure 2A–2C).

The results of the univariate analysis were reported in the Supplementary Table S2 (available in https://weekly.chinacdc.cn/). The final selected model showed that the arrival time positively correlated with the growth rate of the epidemic [odds ratio (*OR*): 1.03, 95% *CI*: 1.02–1.04]. Subdistricts located in the suburban ring (*OR*: 0.85, 95% *CI*: 0.73–0.98) and outside the suburban ring (*OR*: 0.59, 95% *CI*: 0.49–0.70) were associated with a significantly lower epidemic growth rate (Figure 2D). The residuals did not show significant spatial autocorrelation with Moran's *I* analysis. The results were robust after removing the outliers. We obtained similar results with

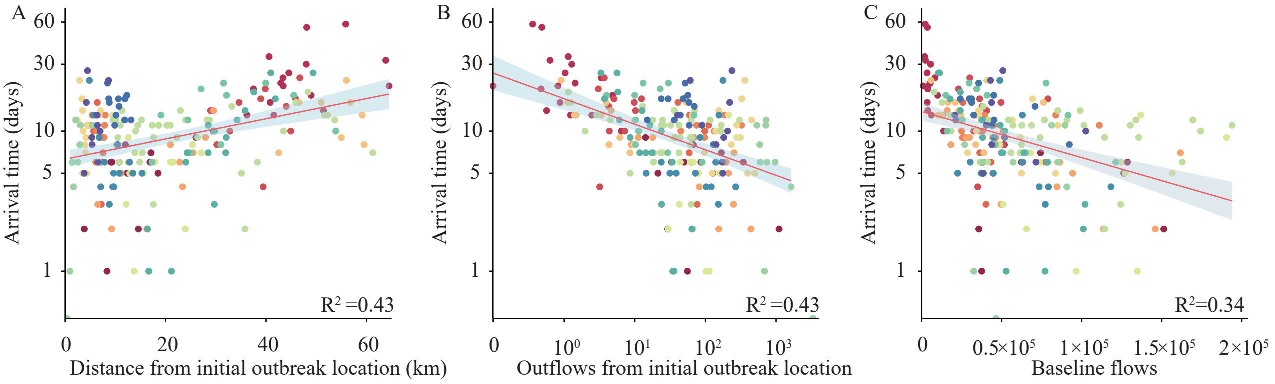

FIGURE 1. Scatter plots of the correlation between epidemic arrival time and (A) geographical distance, (B) effective distance, and (C) baseline flows.

Note: Dots in the scatter plot were colored by different districts.

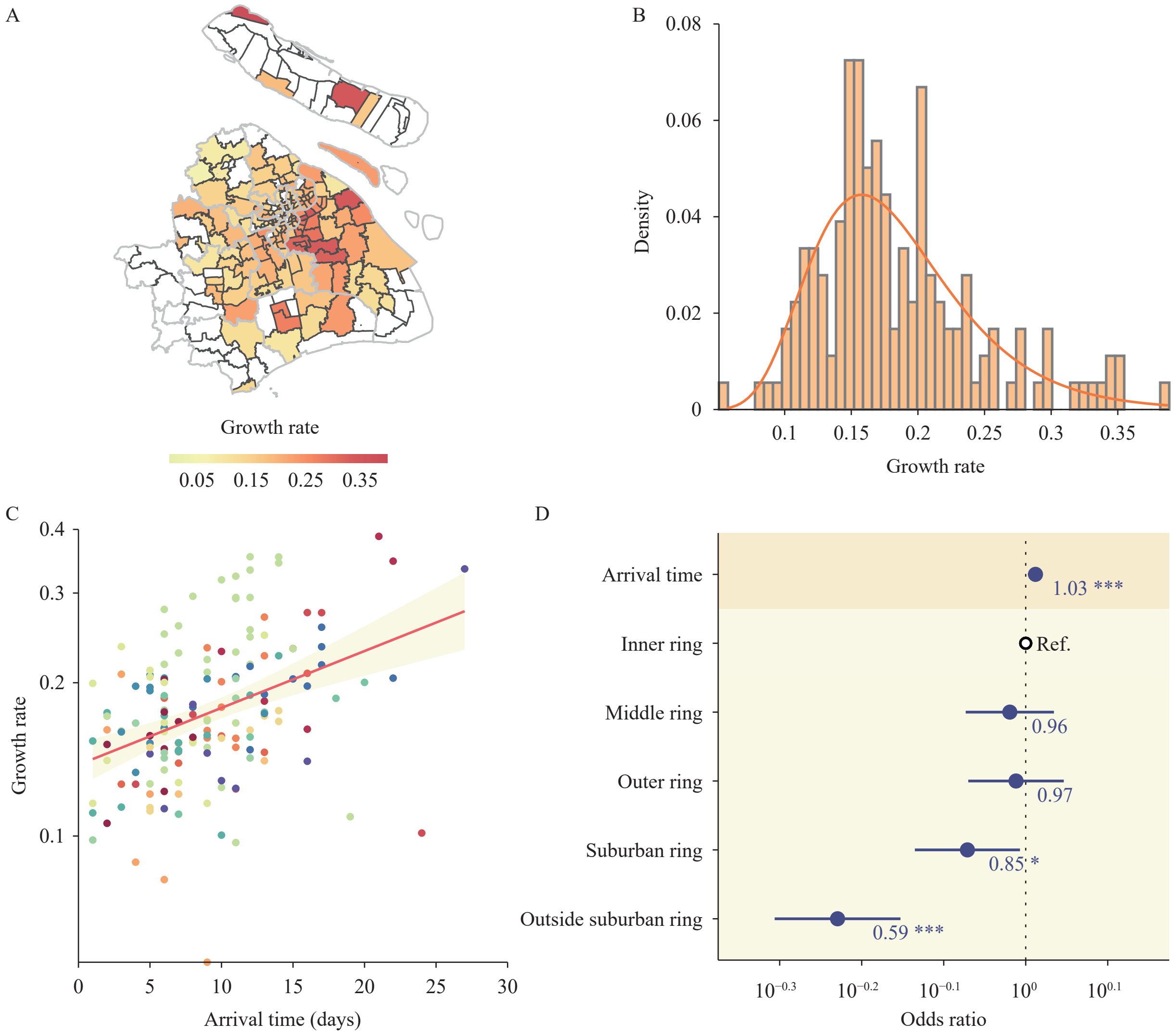

FIGURE 2. Epidemic growth rate and its associated factors. (A) Geographical distribution of growth rates for 158 subdistricts. (B) Distribution of the estimated epidemic growth rate (per day) by subdistrict and fit of a log-normal distribution. (C) Scatter plot of the epidemic growth rate and arrival time. (D) Factors associated with the growth rate.

Note: In panel A, of the 216 subdistricts, 6 subdistricts reporting no infections before the lockdown, 49 subdistricts with an R^2<0.6, and 3 subdistricts with only two data points for estimating their growth rates, were excluded from the regression; the excluded subdistricts are shown in white. In panel C, dots were colored by different districts. In panel D, dots and lines indicate point estimates and 95% confidence intervals of the odds ratio. Odds ratio was calculated as exponentiated regression coefficients. Numbers on the side of the dots indicate the numerical value of the point estimate.

Abbreviation: Ref.=reference category.

* indicates *P*-value<0.05;

** indicates *P*-value<0.01;

*** indicates *P*-value<0.001.

a GEE model (Supplementary Table S3, available in https://weekly.chinacdc.cn/).

As of May 31, 2022, the overall IAR in Shanghai was estimated to be 2.42%. However, the IAR was highly heterogeneous across subdistricts, ranging from 0 to 13.75%. The epidemic arrival time was significantly associated with the IAR. The final selected model showed that the arrival time was negatively correlated with the IAR (*OR*: 0.59, 95% *CI*: 0.46–0.75). Among the investigated demographic characteristics, population density was positively associated with the IAR (*OR*: 1.38, 95% *CI*: 1.20–1.60). Among the socioeconomic characteristics, subdistricts that were farther apart from the initial outbreak location were associated with a significantly lower IAR (*OR*: 0.96, 95% *CI*: 0.95–0.98). GDP at the district level positively correlated with the IAR (*OR*: 1.51, 95% *CI*: 1.23–1.85). Compared to subdistricts located in the inner ring, subdistricts located farther away from the inner ring were significantly associated with lower IARs (*OR* for middle ring: 0.51, 95% *CI*: 0.35–0.73; *OR* for outer ring: 0.43, 95% *CI*: 0.32–0.58; *OR* for suburban ring: 0.16, 95% *CI*: 0.11–0.24; *OR* for outside suburban ring: 0.05, 95% *CI*: 0.03–0.08). Among the vaccine-related covariates, booster coverage for people aged 65 years and above was associated with a significantly lower IAR (*OR*: 0.73, 95% *CI*: 0.55–0.96, Figure 3). Moran's *I* for the residuals showed no significant spatial autocorrelation. The results were robust after removing the outliers, and similar results were obtained with a GEE model (Supplementary Table S4, available in https://weekly.chinacdc.cn/).

DISCUSSION

This study highlights the heterogeneous spread of the 2022 Omicron BA.2 epidemic in Shanghai, and identifies associations between different metrics of spatial spread at the subdistrict level and demographic and socioeconomic characteristics of the population, human mobility patterns, and adopted interventions.

The identified (likely) focus of the outbreak was the cultural activity center of the Shiquan Subdistrict in Putuo District. However, we could not rule out the possibility that the Omicron outbreak might have

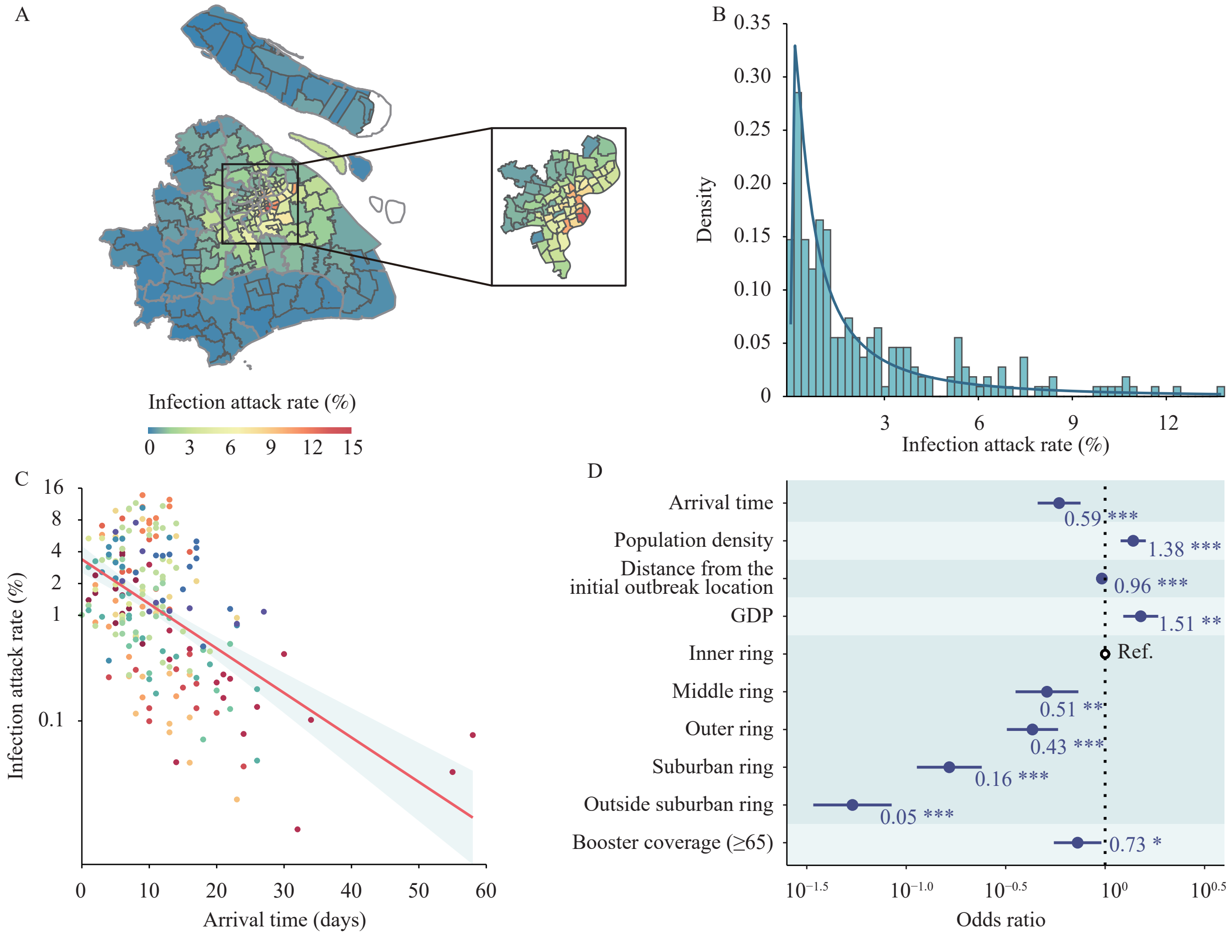

FIGURE 3. Infection attack rate and its associated factors. (A) Geographical distribution of the infection attack rates at the subdistrict level as of May 31, 2022. (B) Distribution of the infection attack rate by subdistrict and fit of a log-normal distribution. (C) Scatter plot of the infection attack rate and arrival time. (D) Factors associated with the infection attack rate.
Note: In panel C, dots were colored by different districts. In panel D, dots and lines indicate point estimates and 95% confidence intervals of the odds ratio. Odds ratio was calculated as exponentiated regression coefficients. Numbers on the side of the dots indicate the numerical value of the point estimates.
Abbreviation: GDP=gross domestic product; Ref.=reference category.
* indicates *P*-value<0.05;
** indicates *P*-value<0.01;
*** indicates *P*-value<0.001.

originated from multiple sources that resulted in simultaneous transmission chains prior to the identification of the first local transmission event.

Our findings suggest that the subdistricts with stronger connections to the initial outbreak location had higher chances of being reached by the epidemic early on, which is consistent with observations for the 2009 H1N1 influenza pandemic and 2003 SARS epidemic (*2*). The epidemic growth rate was positively associated with the arrival time of the epidemic, suggesting that the targeted interventions implemented in high-risk areas were insufficient to slow down transmission (*3*).

Human mobility is generally considered to be key in determining the risk of infection and the spread of epidemics (*4–5*). However, in our multivariate regression models, we found that pre-epidemic population flows were not significantly associated with the IAR or growth rate. This could be explained by its strong collinearity with the epidemic arrival time, which ultimately had a strong impact on determining the type and timing of adoption of control measures (*6*).

Subdistricts with a higher GDP were found to have a higher IAR, consistent with a previous study (*7*). This indicates that subdistricts with a higher GDP trend to have more factories and enterprises, causing more gathering and higher risk of transmission accordingly.

Initially, the outbreak spread in and around the inner ring. Previous literature also found that the COVID-19 pandemic in the United States was characterized by a geographically localized mosaic of transmission along an urban-rural gradient (*8–9*), suggesting that geographic distance may play an important role in SARS-CoV-2 spread. Finally, the public health impact of COVID-19 vaccines has already been widely discussed in the literature (*10–13*) and our study confirms previous evidence.

Our study suffers from limitations that are rooted in the uncertainty and fragmentary nature of publicly available sources, such as a high level of missing data for key variables, such as the date of symptom onset. Additionally, the population flows were provided by China Unicom and thus may suffer from the limitation intrinsic of mobile phone data. Moreover, we cannot exclude the possibility that there are other potential risk factors that were not considered in our study (e.g., housing conditions and meteorological factors). Meteorological factors may play an important role to explain the heterogeneity in the temporal and spatial spread of infectious diseases, but we did not include them here as the variation may be very limited across the small study location and the short study period. Finally, this study does not provide causal relationships, but only provides associations between different metrics of the epidemic spread with a set of indicators.

In conclusion, this study provides a quantitative description of the spatiotemporal spread of the Omicron BA.2 variant in Shanghai at the subdistrict level. Our findings highlight the role of the geographical structure of the city, human mobility, socioeconomic characteristics of the population, and adopted interventions in shaping the dynamics of the epidemic. Disentangling these factors might contribute to a deeper understanding the transmission dynamics and ecology of COVID-19 and guide the design of monitoring and management strategies.

Funding: Supported by the Key Program of the National Natural Science Foundation of China (82130093 to H.Y.) and Shanghai Rising-Star Program (22QA1402300 to J.Z.).

doi: 10.46234/ccdcw2023.018

Corresponding authors: Juanjuan Zhang, zhangjuan@fudan.edu.cn; Hongjie Yu, yhj@fudan.edu.cn.

---

[1] School of Public Health, Fudan University, Key Laboratory of Public Health Safety, Ministry of Education, Shanghai Municipality, China; [2] Laboratory for Computational Epidemiology and Public Health, Department of Epidemiology and Biostatistics, Indiana University School of Public Health, Bloomington, IN, USA; [3] Shanghai Institute of Infectious Disease and Biosecurity, Fudan University, Shanghai Municipality, China.

Submitted: October 27, 2022; Accepted: January 28, 2023

REFERENCES

1. Chen ZY, Deng XW, Fang LQ, Sun KY, Wu YP, Che TL, et al. Epidemiological characteristics and transmission dynamics of the outbreak caused by the SARS-CoV-2 Omicron variant in Shanghai, China: a descriptive study. Lancet Reg Health West Pac 2022;29:100592. http://dx.doi.org/10.1016/j.lanwpc.2022.100592.
2. Brockmann D, Helbing D. The hidden geometry of complex, network-driven contagion phenomena. Science 2013;342(6164):1337 – 42. http://dx.doi.org/10.1126/science.1245200.
3. Hay JA, Kissler SM, Fauver JR, Mack C, Tai CG, Samant RM, et al. Quantifying the impact of immune history and variant on SARS-CoV-2 viral kinetics and infection rebound: a retrospective cohort study. Elife 2022;11:e81849. http://dx.doi.org/10.7554/eLife.81849.
4. Stoddard ST, Morrison AC, Vazquez-Prokopec GM, Soldan VP, Kochel TJ, Kitron U, et al. The role of human movement in the transmission of vector-borne pathogens. PLoS Negl Trop Dis 2009;3(7):e481. http://dx.doi.org/10.1371/journal.pntd.0000481.
5. Doorley R, Berke A, Noyman A, Alonso L, Ribó J, Arroyo V, et al. Mobility and COVID-19 in andorra: country-scale analysis of high-resolution mobility patterns and infection spread. IEEE J Biomed Health Inform 2022;26(1):183 – 93. http://dx.doi.org/10.1109/JBHI.

2021.3121165.

6. Kraemer MUG, Yang CH, Gutierrez B, Wu CH, Klein B, Pigott DM, et al. The effect of human mobility and control measures on the COVID-19 epidemic in China. Science 2020;368(6490):493 – 7. http://dx.doi.org/10.1126/science.abb4218.
7. Liu SR, Qin YC, Xie ZX, Zhang JF. The spatio-temporal characteristics and influencing factors of COVID-19 spread in Shenzhen, China-an analysis based on 417 cases. Int J Environ Res Public Health 2020;17(20):7450. http://dx.doi.org/10.3390/ijerph17207450.
8. Susswein Z, Valdano E, Brett T, Rohani P, Colizza V, Bansal S. Ignoring spatial heterogeneity in drivers of SARS-CoV-2 transmission in the US will impede sustained elimination. medRxiv 2021. http://dx.doi.org/10.1101/2021.08.09.21261807.
9. Souch JM, Cossman JS, Hayward MD. Interstates of infection: preliminary investigations of human mobility patterns in the COVID-19 pandemic. J Rural Health 2021;37(2):266 – 71. http://dx.doi.org/10.1111/jrh.12558.
10. Tan ST, Park HJ, Rodríguez-Barraquer I, Rutherford GW, Bibbins-Domingo K, Schechter R, et al. COVID-19 vaccination and estimated public health impact in California. JAMA Netw Open 2022;5(4):e228526. http://dx.doi.org/10.1001/jamanetworkopen.2022.8526.
11. Watson OJ, Barnsley G, Toor J, Hogan AB, Winskill P, Ghani AC. Global impact of the first year of COVID-19 vaccination: a mathematical modelling study. Lancet Infect Dis 2022;22(9):1293 – 302. http://dx.doi.org/10.1016/S1473-3099(22)00320-6.
12. Suthar AB, Wang J, Seffren V, Wiegand RE, Griffing S, Zell E. Public health impact of COVID-19 vaccines in the US: observational study. BMJ 2022;377:e069317. http://dx.doi.org/10.1136/bmj-2021-069317.
13. Bubar KM, Middleton CE, Bjorkman KK, Parker R, Larremore DB. SARS-CoV-2 transmission and impacts of unvaccinated-only screening in populations of mixed vaccination status. Nat Commun 2022;13(1):2777. http://dx.doi.org/10.1038/s41467-022-30144-7.

SUPPLEMENTARY MATERIAL

Generalized Linear Mixed Effect Model

Arrival time. We built a generalized linear mixed effect model (GLMM) to estimate the proportion of variance in the response variables attributable to intra- and inter-district variation. For the arrival time, we used a GLMM with random intercept effect and log link function to assess its association with geographical distance from the initial outbreak location. We used the concept of "effective distance" (*1*), wherein the distance between locations depends on the strength of their link; in our case, the strength of the link is measured as the outflows from initial outbreak location.

Epidemic growth rate. Similarly, we used a GLMM with random intercept, random slope, and log link function to explore whether and to what extent the arrival time correlates with the epidemic growth rate, while controlling for other covariates. To select which explanatory variables to include in the final model, we first used univariate regression for candidate variable selection, then we run multivariate regressions. Finally, we performed a forward stepwise model selection based on Akaike's Information Criterion (AIC) and likelihood ratio test.

The specification of the final GLMM for the epidemic growth rate is the following:

$$g\left(\mu_{ij}\right) = \alpha + \beta_1 arrival\_time_{ij} + \beta_{2j} ring_{ij} + u_j$$

where g is a log link function; i represents the subdistrict; j represents the district; α represents the intercept; $arrival\_time_{ij}$ and $ring_{ij}$ denote the fixed effects of the arrival time and ring where the subdistrict is located; u_j represents the district-specific random intercept effects; β_{2j} represents the district-specific random slope effects; and $\mu_{ij} = E\left(Y_{ij} \middle| u_j, \beta_{2j}\right)$ is the mean of the response variable (i.e., the epidemic growth rate) Y_{ij} for a given value of the random effects.

Infection attack rate. To explore driving factors associated with the infection attack rate, we used the same GLMM. After model selection, the specification of the final GLMM for IAR is the following:

$$g\left(\mu_{ij}\right) = \alpha + \beta_{1j} arrival\_time_{ij} + \beta_2 density_{ij} + \beta_{3j} ring_{ij} + \beta_4 distance_{ij} + \beta_5 GDP_{ij} + \beta_6 booster\_65_{ij} + u_j$$

where g is a log link function; i represents the subdistrict; j represents the district; α represents the intercept; $arrival\_time_{ij}$, $density_{ij}$, $ring_{ij}$, $distance_{ij}$, GDP_{ij}, and $\mathrm{booster\_65_{ij}}$ denote the fixed effects of the arrival time, population density, ring where the subdistrict is located, distance from the initial outbreak location, GDP, and booster vaccination coverage of people aged 65 years and above; u_j represents the district-specific random intercept effects; β_{1j} and β_{3j} represents the district-specific random slope effects; and $\mu_{ij} = E\left(Y_{ij} \middle| u_j, \beta_{1j}, \beta_{3j}\right)$ is the mean of the response variable (i.e., the infection attack rate) Y_{ij} for a given value of the random effects.

Observations with a Cook's Distance greater than 20 times the mean value were considered outliers and excluded from the analysis. Odd ratios were calculated by exponentiating the coefficients and confidence interval from the regression results. Diagnostics were performed to assess regression assumptions.

Generalized Estimating Equation Model

In addition to the GLMM, we also built a generalized estimating equation (GEE) model to regress the epidemic growth rate and infection attack rate. The GEE model relies on a similar specification of the initial GLM fitting, but with no random effects. To further account for spatial clustering and possible correlation structure, GEE uses u_j to define the clustering structure of the data with a working correlation matrix that defines the correlation within each cluster (i.e., district). We provide the results for the exchangeable correlation matrix, but independent and unstructured matrices were explored as well and gave very similar results.

SUPPLEMENTARY TABLE S1. Definition and data sources for potential risk factors.

Type	Factors	Level	Data source
Demographic characteristics*			
	1. Population density (×1,000 people/km^2)	Subdistrict	6th and 7th Census (*2*–*3*)
	2. Proportion of people aged 65 years old and over (%)	Subdistrict	6th and 7th Census (*2*–*3*)
	3. Ratio of population with household registration to the effective population (%)	Subdistrict	Shanghai Statistics Year Book (*4*)
Socioeconomic characteristics			
	4. Distance from the initial outbreak location, i.e., cultural activity center in Shiquan Subdistrict of Putuo District (km)	Subdistrict	Amap (*5*)
	5. Gross domestic product (GDP) (×100 million CNY)	District	Shanghai Statistics Year Book (*4*)
	6. Coverage of green area (%)	District	Shanghai Statistics Year Book (*4*)
	7. Ring where the subdistrict is located ● Inner ring: subdistricts with more than half of the area within the Inner-city Elevated Beltway; ● Middle ring: subdistricts between the Inner-city Elevated Beltway and the Middle Ring Road; ● Outer ring: subdistricts between the Middle Ring Road and the Outer Ring Road, i.e., S20; ● Suburban ring: subdistricts between the S20 Road and the Highway around Shanghai City, i.e., G1501; ● Outside the suburban ring: subdistricts outside the G1501 Road	Subdistrict	Public sources
Human behavior†			
	8. Baseline flows during pre-epidemic (×1,000 trips): daily average population flows (inflows, outflows and inner flows) for a given subdistrict in the last week of February, i.e., between February 21 and February 27, 2022.	Subdistrict	China Unicom (*6*)
	9. Outflows from the initial outbreak location (i.e., Shiquan Subdistrict) to other 215 subdistricts during pre-epidemic (×1,000 trips): daily average outflows between February 21 and February 27, 2022	Subdistrict	China Unicom (*6*)
Vaccine and non-pharmaceutical interventions			
	10. Vaccine coverage (%)§ ● Primary vaccination coverage of total population ● Booster vaccination coverage of total population ● Primary vaccination coverage of people aged 65 years old and over ● Booster vaccination coverage of people aged 65 years old and over	Subdistrict	Public sources and internal report
	11. Whether a given subdistrict was classified as high-risk area or not, during grid management phase between March 16 and March 27, 2022	Subdistrict	Public sources
	12. Lockdown time of eastern and western Shanghai, defined as subdistricts east and west of the Huangpu River ● Eastern Shanghai: March 28 ● Western Shanghai: April 1	Subdistrict	Public sources
	13. Reduction in daily population flows after lockdown (%): the subtraction of daily average flows during early lockdown (between April 1 and April 7, 2022) from the baseline flows and the division by the baseline	Subdistrict	China Unicom[a] (*6*)

Abbreviation: CNY=Chinese Yuan.

* Subdistrict-level population data after 2017 were derived from the 7th National Census of China and the latest reports by local authorities. For the subdistricts with unavailable population data after 2017, the subdistrict-level population data for 2020 were inferred from the population size of each district in 2020 and the population proportion of each subdistrict in the Sixth National Census in 2010.

† The population flow data is provided by one of the largest national mobile carriers in China, China Unicom, and is aggregated based on all users' mobile phone activity records across the city, including geographic location. We then aggregated the daily inflows, outflows, and internal flows at the subdistrict level.

§ The numerator is vaccinated individuals, and the denominator is census population. If floating population who was vaccinated was counted in the numerator, it may result in coverage exceeding 100%. Besides, census population for some subdistricts is not up to date, possibly leading to overestimation of coverage. Thus, the coverage would be truncated to 100%, if exceeding 100%.

SUPPLEMENTARY TABLE S2. Univariate regression for growth rate and infection attack rate.

Effect	Epidemic growth rate			Infection attack rate (%)		
	Estimate	**Pr(>|z|)**	***95% CI***	**Estimate**	**Pr(>|z|)**	***95% CI***
Population density	1.01	<0.001***	(1.003, 1.01)	2.16	<0.001***	(1.95, 2.39)
Proportion of people aged ≥65	1.07	0.271	(0.95, 1.20)	0.99	0.140	(0.97, 1.004)
Ratio of population with household registration to the effective population	1.00	0.918	(0.93, 1.06)	2.05	<0.001***	(1.67, 2.52)
Distance from initial outbreak location	0.91	0.036*	(0.83, 0.99)	0.93	<0.001***	(0.92, 0.94)
GDP	1.03	0.591	(0.92, 1.17)	2.23	0.050	(1.08, 4.60)
Coverage of green area	1.00	0.763	(0.98, 1.03)	0.93	0.401	(0.81, 1.08)
Ring where the subdistrict is located						
Inner ring	Ref	–	–	Ref	–	–
Middle ring	0.94	0.373	(0.82, 1.08)	0.46	0.009**	(0.30, 0.72)
Outer ring	0.94	0.424	(0.81, 1.09)	0.40	0.005**	(0.26, 0.63)
Suburban ring	0.82	0.021*	(0.70, 0.97)	0.15	<0.001***	(0.09, 0.24)
Outside suburban ring	0.61	<0.001***	(0.50, 0.74)	0.05	<0.001***	(0.03, 0.08)
Baseline flows	1.02	0.593	(0.95, 1.10)	1.86	<0.001***	(1.53, 2.27)
Outflows from initial outbreak location	1.04	0.089	(0.99, 1.08)	1.54	<0.001***	(1.39, 1.72)
Primary coverage of total population	0.99	<0.001***	(0.99, 0.996)	0.44	0.074	(0.18, 1.08)
Booster coverage of total population	0.99	<0.001***	(0.98, 0.996)	0.11	<0.001***	(0.06, 0.22)
Primary coverage of people aged ≥65	1.00	0.381	(1.00, 1.00)	0.81	0.370	(0.52, 1.26)
Booster coverage of people aged ≥65	1.00	0.726	(0.99, 1.00)	0.74	0.150	(0.50, 1.11)
High-risk area	0.93	0.141	(0.85, 1.02)	1.70	<0.001***	(1.29, 2.25)
Lockdown time						
March 28	–	–	–	Ref	–	–
April 1	–	–	–	4.53	<0.001***	(2.35, 8.76)
Reduction in flows after lockdown	–	–	–	1.05	<0.001***	(1.04, 1.07)
Arrival time	1.02	<0.001***	(1.01, 1.03)	0.53	0.004**	(0.37, 0.75)

Abbreviation: GDP=gross domestic product; *CI*=confidence intervals; Ref=reference.
* *P*<0.05;
** *P*<0.01;
*** *P*<0.001.

SUPPLEMENTARY TABLE S3. Generalized estimating equation model for growth rate.

Effect	Exchangeable			Independence			Unstructured		
	Estimate	**Pr(>|z|)**	***95% CI***	**Estimate**	**Pr(>|z|)**	***95% CI***	**Estimate**	**Pr(>|z|)**	***95% CI***
Intercept	0.13	<0.001***	(0.12, 0.15)	0.13	<0.001***	(0.12, 0.15)	0.13	<0.001***	(0.12, 0.15)
Arrival time	1.03	<0.001***	(1.02, 1.04)	1.03	<0.001***	(1.02, 1.04)	1.03	<0.001***	(1.02, 1.04)
Ring where the subdistrict is located									
Inner ring	Ref	–	–	Ref	–	–	Ref	–	–
Middle ring	1.00	0.986	(0.88, 1.14)	1.00	0.983	(0.88, 1.14)	1.00	0.985	(0.88, 1.14)
Outer ring	1.05	0.253	(0.94, 1.26)	1.09	0.254	(0.94, 1.26)	1.09	0.253	(0.94, 1.26)
Suburban ring	1.01	0.865	(0.90, 1.14)	1.01	0.869	(0.90, 1.14)	1.01	0.866	(0.90, 1.14)
Outside suburban ring	0.79	0.061	(0.61, 1.01)	0.79	0.060	(0.61, 1.01)	0.79	0.061	(0.61, 1.01)

Note: Total *N*=158. d*f*=152.
Abbreviation: *CI*=confidence intervals; Ref=reference.
* *P*<0.05;
** *P*<0.01;
*** *P*<0.001.

SUPPLEMENTARY TABLE S4. Generalized estimating equation model for infection attack rate.

Effect	Exchangeable			Independence			Unstructured		
	Estimate	**Pr(>|z|)**	**95% *CI***	**Estimate**	**Pr(>|z|)**	**95% *CI***	**Estimate**	**Pr(>|z|)**	**95% *CI***
Intercept	0.01	<0.001***	(0, 0.03)	0.01	<0.001***	(0.01, 0.03)	0.01	<0.001***	(0, 0.04)
Arrival time	0.75	0.013*	(0.59, 0.94)	0.74	0.009**	(0.59, 0.93)	0.73	0.008**	(0.58, 0.92)
Population density	1.51	0.001**	(1.20, 1.91)	1.57	<0.001***	(1.26, 1.96)	1.65	<0.001***	(1.29, 2.10)
Distance from the initial outbreak location	1.01	0.653	(0.98, 1.03)	1.01	0.536	(0.98, 1.03)	1.01	0.442	(0.98, 1.04)
GDP	1.35	<0.001***	(1.17, 1.56)	1.35	<0.001***	(1.20, 1.53)	1.33	0.001**	(1.13, 1.58)
Ring where the subdistrict is located									
Inner ring	Ref	–	–	Ref	–	–	Ref	–	–
Middle ring	0.45	<0.001***	(0.34, 0.59)	0.42	<0.001***	(0.32, 0.56)	0.44	<0.001***	(0.31, 0.63)
Outer ring	0.46	<0.001***	(0.36, 0.58)	0.43	<0.001***	(0.34, 0.55)	0.44	<0.001***	(0.34, 0.58)
Suburban ring	0.18	<0.001***	(0.13, 0.24)	0.17	<0.001***	(0.13, 0.23)	0.17	<0.001***	(0.12, 0.24)
Outside suburban ring	0.06	<0.001***	(0.04, 0.09)	0.05	<0.001***	(0.04, 0.08)	0.06	<0.001***	(0.04, 0.09)
Booster coverage of people aged ≥ 65 years old	0.67	0.001**	(0.53, 0.84)	0.67	0.002**	(0.53, 0.86)	0.68	0.002**	(0.54, 0.87)

Note: Total *N*=216. d*f*=198.

Abbreviation: *CI*=confidence intervals; Ref=reference.

* *P*<0.05;

** *P*<0.01;

*** *P*<0.001.

SUPPLEMENTARY FIGURE S1. Geographic division of eastern and western Shanghai.

Note: Eastern and western Shanghai are naturally separated by the Huangpu River (blue layer). Specifically, eastern Shanghai contained the districts of Pudong New Area, Fengxian, Jinshan, Chongming, as well as partial Minhang and Songjiang; while the rest areas were grouped into western Shanghai.

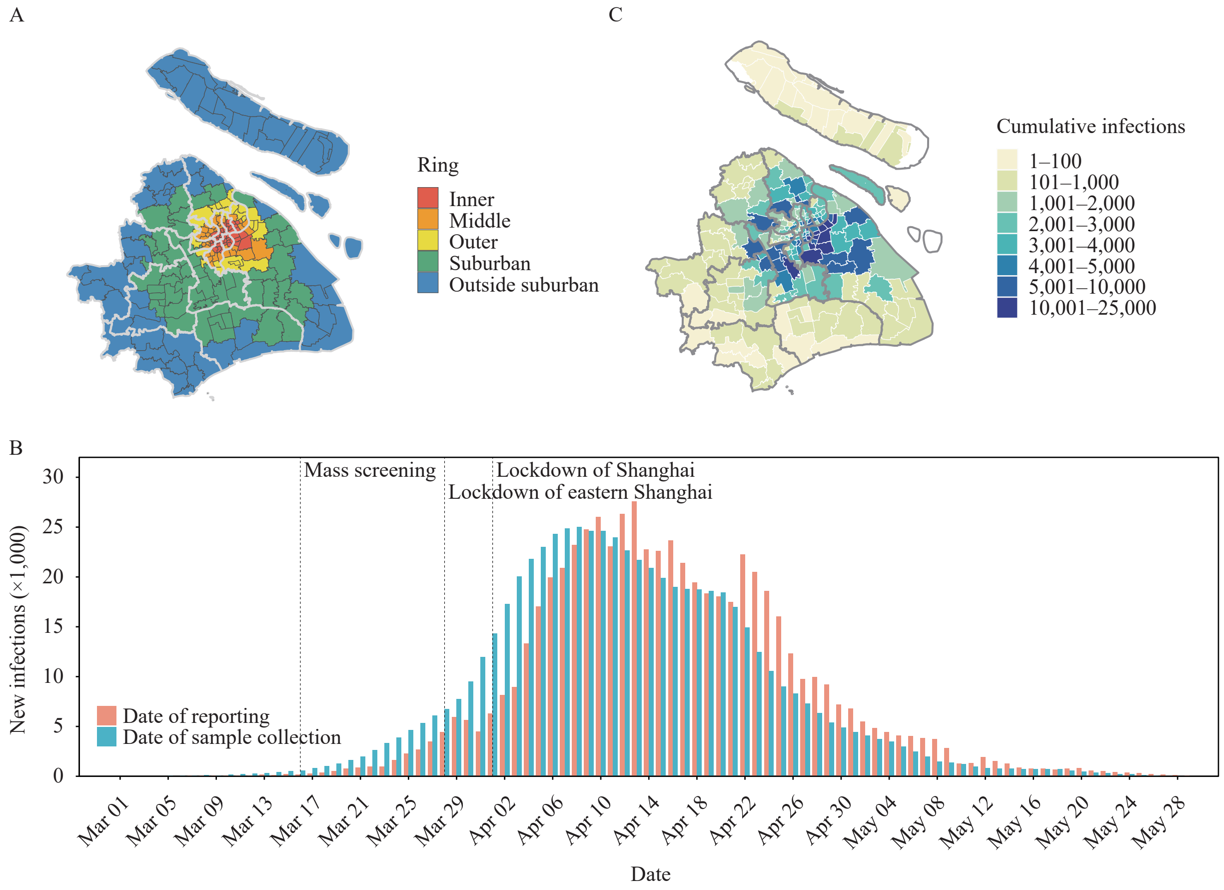

SUPPLEMENTARY FIGURE S2. Temporal dynamics and geographical distribution of confirmed severe acute respiratory syndrome coronavirus 2 (SARS-CoV-2) infections. (A) Visualization of the ring where the subdistrict is located. (B) Geographical distribution of confirmed SARS-CoV-2 infections at the subdistrict level. (C) Daily number of new confirmed infections by date of reporting and by date of sample collection.

Note: Shanghai is divided into 16 districts (light grey boundary) and 216 subdistricts (black boundary) shown in panel A. The colored area corresponds to the ring where the subdistrict is located.

REFERENCES

1. Brockmann D, Helbing D. The hidden geometry of complex, network-driven contagion phenomena. Science 2013;342(6164):1337 – 42. http://dx.doi.org/10.1126/science.1245200.
2. Office of the Leading Group of the State Council for the Seventh National Population Census. China population census yearbook 2020. Beijing: China Statistics Press. 2022. https://book.kongfz.com/13826/5510107594/. (In Chinese).
3. Population Census Office Under the State Council Department of Population, Employment Statistics National Bureau of Statistics. Tabulation on the 2010 population census of the People's Republic of China. Beijing: China Statistics Press. 2012. https://book.kongfz.com/351691/4922881913/. (In Chinese).
4. Shanghai Municipal Bureau of Statistics, Survey office of the National Bureau of Statistics in Shanghai. Shanghai Statistical Yearbook 2021. Beijing: China Statistics Press. 2021. https://book.kongfz.com/8654/4665739962/. (In Chinese).
5. Amap. https://ditu.amap.com/. [2022-6-29]. (In Chinese).
6. SmartSteps. SmartSteps. http://www.smartsteps.com/. [2022-6-29]. (In Chinese).

Preplanned Studies

Modeling the Prediction on the Efficacy of a Homologous Third Dose of CoronaVac Against SARS-CoV-2 Omicron BA.1, BA.2, BA.2.12.1, and BA.4/5 — China, 2020–2021

Xinhua Chen[1]; Xufang Bai[1]; Xinghui Chen[1]; Nan Zheng[1]; Juan Yang[1]; Juanjuan Zhang[1,2]; Hongjie Yu[1,3,#]

Summary

What is already known about this topic?

Previous studies have reported vaccine efficacy or effectiveness against severe acute respiratory syndrome coronavirus 2 (SARS-CoV-2) Omicron subvariants for several vaccine platforms. However, there are currently few data on estimates of inactivated platform coronavirus disease 2019 (COVID-19) vaccines, especially against the globally dominant subvariant — Omicron BA.5.

What is added by this report?

The study predicts vaccine efficacy against four Omicron subvariants — Omicron BA.1, BA.2, BA.2.12.1, and BA.4/5 — after vaccination with a homologous third dose of CoronaVac across clinical endpoints and age groups.

What are the implications for public health practice?

The results suggest that CoronaVac-elicited immunity may not provide adequate protection against Omicron subvariants after the homologous third dose, and a heterologous booster and Omicron-specific vaccination may be alternative strategies.

The severe acute respiratory syndrome coronavirus 2 (SARS-CoV-2) Omicron variant, a designated variant of concern (VOC) by the World Health Organization (WHO), was first identified in November 2021 in South Africa (*1*). Three major subvariants, BA.1, BA.2, and BA.3, were identified nearly simultaneously. Soon after its discovery, BA.1 rapidly emerged to become the dominant subvariant worldwide. Gradually, BA.2 and its constituent subvariants, such as BA.2.12.1, overtook BA.1 as the dominant variant worldwide. More recently, two new subvariants, BA.4 and BA.5, were first discovered in South Africa. As of October 1, 2022, the Omicron BA.5 subvariant has been observed in 139 countries across all six WHO regions and has become a globally dominant subvariant due to its substantial growth advantages and faster spread compared to previous subvariants (*2*). Preliminary data suggest that highly divergent mutations in the spike protein of Omicron may be associated with a high level of humoral immune evasion.

There are limited efficacy or effectiveness data on the Omicron subvariants for the CoronaVac inactivated vaccine, and the duration of protection after a homologous inactivated vaccine booster dose has not been fully explored. Given the extensive resources and time required to identify and distinguish variants in vaccine trials, statistical models were used to predict CoronaVac-specific efficacy against Omicron BA.1, BA.2, BA.2.12.1, and BA.4/5 across three clinical endpoints — infection, symptomatic coronavirus disease 2019 (COVID-19), and severe COVID-19 — 28 days and 6 months after a homologous third dose.

Age-specific neutralizing data was extracted from a randomized, double-blind, placebo-controlled, phase 1/2 clinical trial of CoronaVac among healthy adults aged 18 years and older (*3*) (Supplementary Table S1, available in https://weekly.chinacdc.cn/). Briefly, in the clinical trial, blood samples were obtained from a group of predefined participants who were vaccinated with a homologous third dose of 3 μg of CoronaVac 28 days or 6 months after two primary series doses of CoronaVac. Fold change data on neutralizing antibodies against SARS-CoV-2 Omicron subvariants compared to the prototype strain were extracted from a published study, which separately estimated the reduction fold of geometric mean antibody titers (GMTs) through a live virus neutralization assay (*4*) (Supplementary Table S2, available in https://weekly.chinacdc.cn/).

Following the models by Khoury et al. (*5*), the vaccine protection of CoronaVac, for 28 days and 6 months after the homologous third dose with the relationship between neutralizing antibody levels, and vaccine efficacy were predicted. Model details and parameters are summarized in the Supplementary Table S3 (available in https://weekly.chinacdc.cn/). All statistical analyses were performed using R software (version 4.0.1, R Core Team, Vienna, Austria).

For vaccine-induced protection against infection caused by four Omicron subvariants, the predicted efficacies of CoronaVac were very low even with homologous booster doses, with less than 30% and 10% of the predicted efficacy against Omicron subvariants 28 days and 6 months after a homologous third dose, respectively. Age did not significantly affect the predicted efficacy against virus infection over time in the model results (Figure 1).

For protection from symptomatic illness from

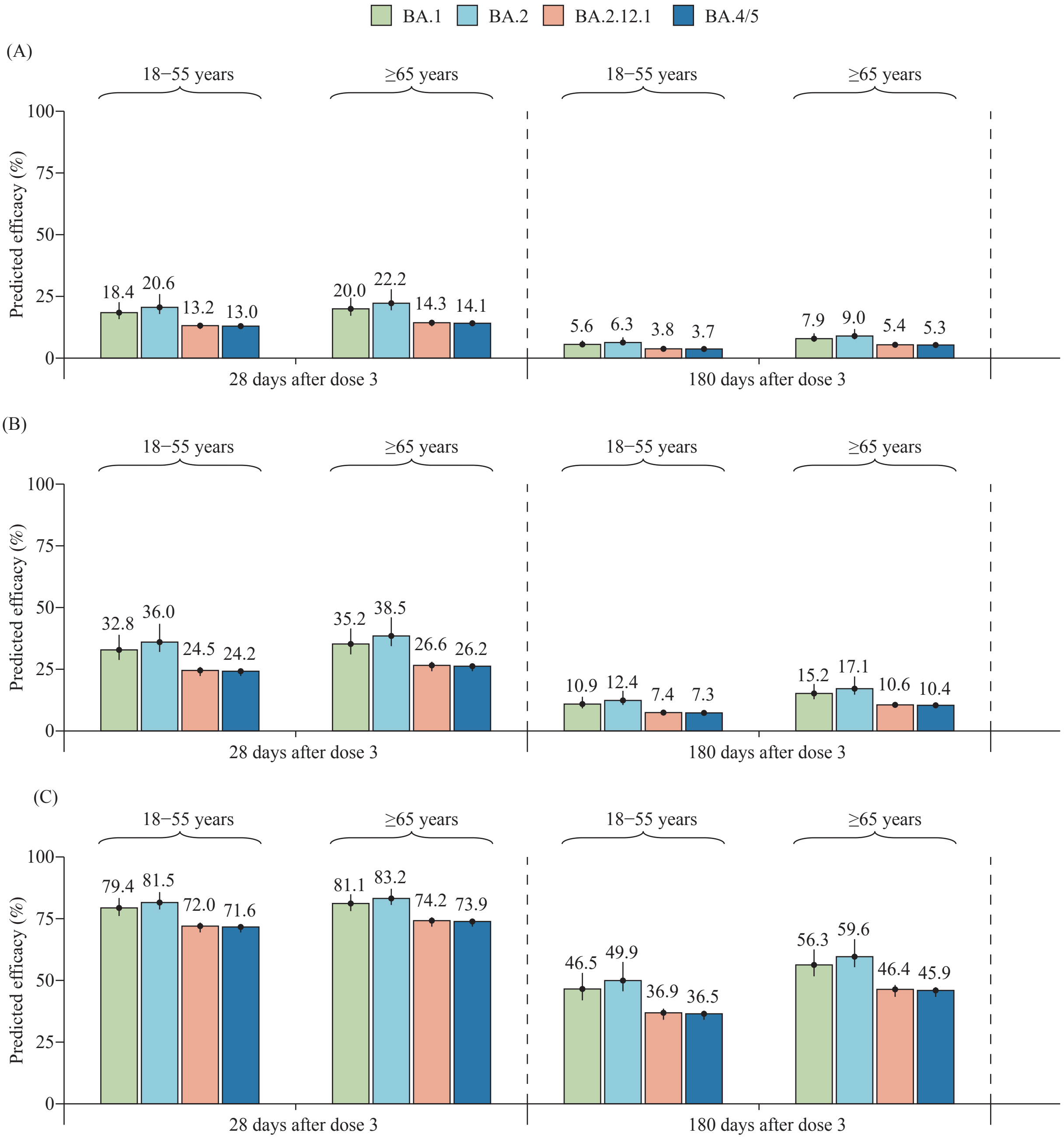

FIGURE 1. Predicted efficacy of CoronaVac against SARS-CoV-2 Omicron subvariants across three clinical endpoints. (A) SARS-CoV-2 infection; (B) Symptomatic COVID-19; (C) Severe COVID-19.

Note: The number on the top of the bar represents the predicted efficacy, and the vertical line represents the 95% confidence interval.

Abbreviation: COVID-19=coronavirus disease 2019; SARS-CoV-2=severe acute respiratory syndrome coronavirus 2.

Omicron infection, the predicted efficacies against BA.4/5 were 24.2% [95% confidence interval (*CI*): 22.3%–25.2%] and 26.2% (95% *CI*: 24.2%–27.3%) for younger adults (18–64 years old) and older adults (≥65 years old) 28 days after the homologous third dose, respectively. Predicted efficacies against BA.4/5 were 7.3% (95% *CI*: 6.6%–7.7%) for younger adults and 10.4% (95% *CI*: 9.4%–10.9%) for older adults 6 months after the homologous third dose (Figure 1). Compared with other Omicron subvariants, the predicted efficacies against BA.4/5 were similar to those against BA.2.12.1 but lower than those against BA.1 and BA.2 after the homologous third dose of CoronaVac. For severe COVID-19, the predicted efficacies against Omicron BA.4/5 were 71.6% (95% *CI*: 69.4%–72.7%) and 36.5% (95% *CI*: 34.0%–37.7%) 28 days and 6 months after the homologous third dose for young adults, respectively. For older adults, the predicted efficacies were 73.9% (95% *CI*: 71.8%–74.9%) and 45.9% (95% *CI*: 43.3%–47.2%) 28 days and 6 months after the homologous third dose, respectively, with no significant difference compared with younger adults (Figure 1).

DISCUSSION

The study predicted the efficacy against the Omicron BA.1, BA.2, BA.2.12.1, and BA.4/5 subvariants after a homologous third dose of CoronaVac across three clinical endpoints. Vaccine protection against infection and symptomatic illness caused by the Omicron subvariants was found to be not adequate, even after a homologous third dose, and that protection was not maintained for 6 months. Although a homologous booster dose of CoronaVac would increase its efficacy to more than 70% for protection from severe illness within one month after a booster, the predicted efficacy from homologous boosting will wane, gradually declining to less than 50% after 6 months.

Compared to the Wuhan-Hu-1 reference genome, the Omicron variant has more than 30 mutations in the spike protein, nearly half of which are in the receptor-binding domain (*6*). This degree of genetic change in such an important part of the virus raised serious concerns about strong immune evasion and significant reductions in vaccine efficacy (*7*). Regarding Omicron subvariants, BA.2.12.1 and BA.4/5 increased evasion of neutralizing antibodies compared with BA.2 and BA.1 (*8*). In plasma from individuals who received an inactivated vaccine (CoronaVac) or receptor binding domain (RBD) protein (ZF2001) booster six months after two doses of CoronaVac, BA.1 and BA.2 showed no significant difference in resistance to neutralization by plasma. However, BA.2.12.1 showed increased immune evasion capability over BA.2, and BA.4/BA.5 exhibited even greater evasion, with the major contributions made from L452R and F486V mutations (*8*–*9*). Such a large degree of immune escape for BA.4/5 may partly verify our predicted results of a lower efficacy, compared to ancestral strains, across all three clinical endpoints.

A previous study reported that the effectiveness of booster vaccination against a documented Omicron BA.2 infection and severe/critical illness in Shanghai Municipality, China, a city with widespread usage of inactivated vaccines, was 18.0% (95% *CI*: 17.0%–18.9%) and 92.8% (95% *CI*: 90.2%–94.7%), respectively. The study also found that a homologous booster dose provided 9 months of >80% protection against more severe outcomes, which was similar to predicted efficacies against Omicron BA.2 in this study (*10*). Another study reported that the effectiveness of three doses of CoronaVac against mild or moderate disease caused by Omicron BA.2 was 32.4%–51.0%, with a relatively wide confidence interval of 8.3%–60.4%, which covered the range of symptomatic estimates of 32.0%–46.0% were used in this study (*11*). Besides, the observed effectiveness among individuals with diabetes or kidney disease against different clinical outcomes caused by BA.2 infection was comparable to the predicted results of this study (*12*–*13*). Of note, such a comparison should be made cautiously due to differences derived from the study methodology, definition of clinical outcomes, characteristics of study participants, and timepoints used to calculate effectiveness/efficacy. However, there are currently few data on the effectiveness against Omicron BA.4/5 of inactivated platform COVID-19 vaccines, which limits comparisons between real-world evidence and our predictions. The efficacy 28 days and 6 months after a homologous third dose of CoronaVac was predicted and it was found that the protective effect against Omicron subvariants was not retained for 6 months due to antibody waning, indicating that a homologous booster of inactivated vaccine may not be a suitable regimen for controlling potential large-scale transmission of the Omicron variant. More recent evidence has shown that heterologous booster vaccination induces strong humoral responses and augments neutralization potency against the Omicron variant. Specifically, a third dose of BNT162b2/Pfizer vaccine given to those who received two primary doses of CoronaVac could provide protective levels of antibodies against Omicron (*14*). A real-world study also revealed that a BNT162b2/Pfizer vaccine booster based on two doses of ChAdOx1 nCoV-19/AstraZeneca can provide 71.4% protection against symptomatic illness caused by infection with the Omicron variant (*15*). In addition, replacing vaccine antigens and accelerating the development of Omicron-specific vaccines may be alternative solutions. For example, the first bivalent COVID-19 booster made by Moderna that targets both the original virus and the Omicron BA.1 variant was approved by regulators in the United Kingdom and the Food and Drug Administration (*16*). Besides, more and more evidence showed that bivalent booster doses are effective in preventing moderate and severe COVID-19 caused by Omicron BA.4/5 infections compared with previous monovalent mRNA vaccine doses only (*17–19*).

The study was subject to at least two limitations. First, only predictions of efficacy for an inactivated vaccine of CoronaVac were made due to limited time-varying neutralization data after boosting doses for other-platform vaccines. Second, predicted estimates need further verification by real-world evidence as more effectiveness data of inactivated vaccines are revealed.

In conclusion, the study provided predictions of vaccine efficacy against the 4 SARS-CoV-2 Omicron subvariants 28 days and 6 months after a homologous third dose of CoronaVac across 3 clinical endpoints. The findings suggest that CoronaVac-elicited immunity may not provide adequate protection after a homologous third dose. Heterologous boosting and vaccination with an Omicron-specific booster may be a viable strategy to protect people from Omicron infection.

Conflicts of interest: H.Y. received research funding from Sanofi Pasteur and Shanghai Roche Pharmaceutical Company; No other conflicts of interest reported.

Acknowledgement: Lance Rodewald from China CDC for language polish.

Funding: Supported by the Key Program of the National Natural Science Foundation of China (82130093) and Shanghai Municipal Science and Technology Major Project (HS2021SHZX001).

doi: 10.46234/ccdcw2023.019

[#] Corresponding author: Hongjie Yu, yhj@fudan.edu.cn.

---

[1] School of Public Health, Fudan University, Key Laboratory of Public Health Safety, Ministry of Education, Shanghai Municipality, China; [2] Shanghai Huashen Institute of Microbes and Infections, Shanghai Municipality, China; [3] Shanghai Institute of Infectious Disease and Biosecurity, Fudan University, Shanghai Municipality, China.

Submitted: November 01, 2022; Accepted: January 28, 2023

REFERENCES

1. WHO. Tracking SARS-CoV-2 variants. 2021. https://www.who.int/activities/tracking-SARS-CoV-2-variants/. [2022-9-15].
2. Gangavarapu K, Latif AA, Mullen JL, Alkuzweny M, Hufbauer E, Tsueng G, et al. Outbreak.info genomic reports: scalable and dynamic surveillance of SARS-CoV-2 variants and mutations. medRxiv 2022. http://dx.doi.org/10.1101/2022.01.27.22269965.
3. Xin QQ, Wu QH, Chen XH, Han BH, Chu K, Song Y, et al. Six-month follow-up of a booster dose of CoronaVac in two single-centre phase 2 clinical trials. Nat Commun 2022;13(1):3100. http://dx.doi.org/10.1038/s41467-022-30864-w.
4. Cheng SSM, Mok CKP, Li JKC, Ng SS, Lam BHS, Jeevan T, et al. Plaque-neutralizing antibody to BA.2.12.1, BA.4 and BA.5 in individuals with three doses of BioNTech or CoronaVac vaccines, natural infection and breakthrough infection. J Clin Virol 2022;156:105273. http://dx.doi.org/10.1016/j.jcv.2022.105273.
5. Khoury DS, Cromer D, Reynaldi A, Schlub TE, Wheatley AK, Juno JA, et al. Neutralizing antibody levels are highly predictive of immune protection from symptomatic SARS-CoV-2 infection. Nat Med 2021;27(7):1205 – 11. http://dx.doi.org/10.1038/S41591-021-01377-8.
6. Han PC, Li LJ, Liu S, Wang QS, Zhang D, Xu ZP, et al. Receptor binding and complex structures of human ACE2 to spike RBD from omicron and delta SARS-CoV-2. Cell 2022;185(4):630 – 40.e10. http://dx.doi.org/10.1016/j.cell.2022.01.001.
7. Cao YL, Wang J, Jian FC, Xiao TH, Song WL, Yisimayi A, et al. Omicron escapes the majority of existing SARS-CoV-2 neutralizing antibodies. Nature 2022;602(7898):657 – 63. http://dx.doi.org/10.1038/s41586-021-04385-3.
8. Cao YL, Yisimayi A, Jian FC, Song WL, Xiao TH, Wang L, et al. BA.2.12.1, BA.4 and BA.5 escape antibodies elicited by Omicron infection. Nature 2022;608(7923):593 – 602. http://dx.doi.org/10.1038/s41586-022-04980-y.
9. Tuekprakhon A, Nutalai R, Dijokaite-Guraliuc A, Zhou DM, Ginn HM, Selvaraj M, et al. Antibody escape of SARS-CoV-2 Omicron BA.4 and BA.5 from vaccine and BA.1 serum. Cell 2022;185(14):2422 – 33.e13. http://dx.doi.org/10.1016/j.cell.2022.06.005.
10. Huang ZY, Xu SF, Liu JC, Wu LL, Qiu J, Wang N, et al. Effectiveness of inactivated and Ad5-nCoV COVID-19 vaccines against SARS-CoV-2 Omicron BA.2 variant infection, severe illness, and death. BMC Med 2022;20(1):400. http://dx.doi.org/10.1186/s12916-022-02606-8.
11. McMenamin ME, Nealon J, Lin Y, Wong JY, Cheung JK, Lau EHY, et al. Vaccine effectiveness of one, two, and three doses of BNT162b2 and CoronaVac against COVID-19 in Hong Kong: a population-based observational study. Lancet Infect Dis 2022;22(10):1435 – 43. http://dx.doi.org/10.1016/S1473-3099(22)00345-0.
12. Cheng FWT, Fan M, Wong CKH, Chui CSL, Lai FTT, Li X, et al. The effectiveness and safety of mRNA (BNT162b2) and inactivated (CoronaVac) COVID-19 vaccines among individuals with chronic kidney diseases. Kidney Int 2022;102(4):922 – 5. http://dx.doi.org/10.1016/j.kint.2022.07.018.
13. Wan EYF, Mok AHY, Yan VKC, Wang BY, Zhang R, Hong SN, et al.

Vaccine effectiveness of BNT162b2 and CoronaVac against SARS-CoV-2 Omicron BA.2 infection, hospitalisation, severe complications, cardiovascular disease and mortality in patients with diabetes mellitus: a case control study. J Infect 2022;85(5):e140 – 4. http://dx.doi.org/10.1016/j.jinf.2022.08.008.

14. HKU MED. HKUMed-CU Medicine joint study finds that third dose of Comirnaty has better protection from COVID-19 variant Omicron. 2021. https://www.med.hku.hk/en/news/press/20211223-hku-cuhk-third-dose-vaccine-omicron. [2022-9-15].
15. Andrews N, Stowe J, Kirsebom F, Toffa S, Rickeard T, Gallagher E, et al. COVID-19 vaccine effectiveness against the omicron (B.1.1.529) variant. N Engl J Med 2022; 386:1532-1546. http://dx.doi.org/10.1056/NEJMoa2119451.
16. U.S. Food & Drug Administration. Moderna COVID-19 vaccines spikevax, moderna COVID-19 vaccine and moderna COVID-19 vaccine, bivalent. 2022. https://www.fda.gov/emergency-preparedness-and-response/coronavirus-disease-2019-covid-19/moderna-covid-19-vaccines. [2022-9-15].
17. Surie D, DeCuir J, Zhu YW, Gaglani M, Ginde AA, Douin DJ, et al. Early estimates of bivalent mRNA vaccine effectiveness in preventing COVID-19-associated hospitalization among immunocompetent adults aged ≥65 Years - IVY network, 18 States, September 8-November 30, 2022. MMWR Morb Mortal Wkly Rep 2022;71(5152):1625 – 30. http://dx.doi.org/10.15585/mmwr.mm715152e2.
18. Tenforde MW, Weber ZA, Natarajan K, Klein NP, Kharbanda AB, Stenehjem E, et al. Early estimates of bivalent mRNA vaccine effectiveness in preventing COVID-19-associated emergency department or urgent care encounters and hospitalizations among immunocompetent adults - VISION network, Nine States, September-November 2022. MMWR Morb Mortal Wkly Rep 2022;71(5152):1616 – 24. http://dx.doi.org/10.15585/mmwr.mm715152e1.
19. Link-Gelles R, Ciesla AA, Fleming-Dutra KE, Smith ZR, Britton A, Wiegand RE, et al. Effectiveness of bivalent mRNA vaccines in preventing symptomatic SARS-CoV-2 infection - increasing community access to testing program, United States, September-November 2022. MMWR Morb Mortal Wkly Rep 2022;71(48):1526 – 30. http://dx.doi.org/10.15585/mmwr.mm7148e1.

SUPPLEMENTARY MATERIAL

SUPPLEMENTARY TABLE S1. Neutralizing antibody dynamics for CoronaVac by time period.

Reference	Vaccine	Age (years)	Neutralization assay	GMTs (95% *CI*)	Neutralizing titers in convalescent individuals (Phase I/II trials)
Xin et al., (*1*)	CoronaVac	18–55	CPE-based microneutralization assay	28 days after the second dose: 49.1 (40.1–60.2) 6 months after the second dose: 6.7 (5.2–8.6) 28 days after a homologous third dose: 143.3 (112.3–182.8) 6 months after a homologous third dose: 36.4 (28.7–46.1)	163.7
		65–85	CPE-based microneutralization assay	28 days after the second dose: 41.2 (34.2–49.6) 6 months after the second dose: 3.4 (2.9–4.1) 28 days after a homologous third dose: 158.5 (96.9–259.2) 6 months after a homologous third dose: 53.2 (39.7–71.1)	163.7

Abbreviation: *CI*=confidence interval.

SUPPLEMENTARY TABLE S2. Fold change in neutralization antibody levels of the Delta and Omicron variants compared to prototype strains.

Vaccine	Type of neutralization assay	Fold change from original study	Data source
CoronaVac	Live virus neutralization assay	BA.1: 8.0 (95% *CI*: 6.2–9.6) BA.2: 7.0 (95% *CI*: 5.2–8.3) BA.2.12.1: 11.8 (95% *CI*: 11.0–13.3) BA.4/5: 12.0 (95% *CI*: 11.4–13.3)	Plaque-neutralizing antibody to BA.2.12.1, BA.4, and BA.5 in individuals with three doses of BioNTech or CoronaVac vaccines, natural infection and breakthrough infection (*2*).

Abbreviation: *CI*=confidence interval.

SUPPLEMENTARY TABLE S3. Model parameters used in the prediction of efficacy

Model structure	LL	AIC	Slope (*k*)	Pooled SD
Fitting protection from symptomatic *vs*. severe COVID-19				
Symptomatic	–	–	3.0 (2.2–4.2)	
Severe	−66.08	138.16	2.94 (2.14–4.04)	0.44
Fitting protection from symptomatic COVID-19 *vs*. SARS-CoV-2 infection				
Infection	−61.10	128.20	2.88 (2.19–3.78)	0.44

Note: "−" means not applied.

Abbreviation: LL=log-likelihood; AIC=Akaike information criterion; SD=standard deviation; COVID-19=coronavirus disease 2019; SARS-CoV-2=severe acute respiratory syndrome coronavirus 2.

REFERENCES

1. Xin QQ, Wu QH, Chen XH, Han BH, Chu K, Song Y, et al. Six-month follow-up of a booster dose of CoronaVac in two single-centre phase 2 clinical trials. Nat Commun 2022;13(1):3100. http://dx.doi.org/10.1038/s41467-022-30864-w.
2. Cheng SSM, Mok CKP, Li JKC, Ng SS, Lam BHS, Jeevan T, et al. Plaque-neutralizing antibody to BA.2.12.1, BA.4 and BA.5 in individuals with three doses of BioNTech or CoronaVac vaccines, natural infection and breakthrough infection. J Clin Virol 2022;156:105273. http://dx.doi.org/10.1016/j.jcv.2022.105273.

Preplanned Studies

A Retrospective Modeling Study of the Targeted Non-Pharmaceutical Interventions During the Xinfadi Outbreak in the Early Stage of the COVID-19 Pandemic — Beijing, China, 2020

Yan Wang[1,&]; Kaiyuan Sun[2,&]; Yang Pan[3,&]; Lan Yi[4]; Da Huo[3]; Yanpeng Wu[4]; Shuaibing Dong[3]; Jinxin Guo[1]; Xiangfeng Dou[3]; Wei Wang[1]; Shuangsheng Wu[3]; Xufang Bai[1]; Hongjie Yu[1,4,#]; Quanyi Wang[3,#]

Summary

What is already known about this topic?

China has repeatedly contained multiple severe acute respiratory syndrome coronavirus 2 (SARS-CoV-2) outbreaks through a comprehensive set of targeted non-pharmaceutical interventions (NPIs). However, the effectiveness of such NPIs has not been systematically assessed.

What is added by this report?

A multilayer deployment of case isolation, contact tracing, targeted community lockdowns, and mobility restrictions could potentially contain outbreaks caused by the SARS-CoV-2 ancestral strain, without the requirement of city-wide lockdowns. Mass testing could further aid in the efficacy and speed of containment.

What are the implications for public health practice?

Pursuing containment in a timely fashion at the beginning of the pandemic, before the virus had the opportunity to spread and undergo extensive adaptive evolution, could help in averting an overall pandemic disease burden and be socioeconomically cost-effective.

Three years into the coronavirus disease 2019 (COVID-19) pandemic, several severe acute respiratory syndrome coronavirus 2 (SARS-CoV-2) variants have emerged with increasing potency in the human population, causing considerable morbidity and mortality worldwide, while Chinese mainland has been able to maintain local containment through an extensive set of targeted non-pharmaceutical interventions (NPIs) (*1*). Here we developed a fully stochastic, spatially structured, agent-based model of SARS-CoV-2 ancestral strain and reconstructed the Beijing Xinfadi outbreak between June 11 and July 10, 2020. This quantitatively assessed the feasibility and prerequisites for containing the virus before it had the opportunity to acquire its high transmissivity and immune-evasive properties. We found that screening for symptoms and among high-risk populations served as an aid in uncovering the cryptic community transmission in the early stages of the outbreak. Effective contact tracing greatly reduces transmission. Targeted community lockdowns and temporal mobility restrictions could slow down the spatial spread of the virus. Mass testing could further improve the speed at which the outbreak is contained. Our analysis suggests that the containment of SARS-CoV-2 ancestral strains is certainly feasible. Early in time measures to stop further spread of the outbreak, prevent mutation of the virus into a more deadly variant are cost-effective and can save lives.

The Beijing Xinfadi Wholesale Market outbreak was initially identified on June 11, 2020, shortly after the successful suppression of the initial wave in Wuhan that ended in March 2020 and caused by the ancestral strain of SARS-CoV-2, with the D614G mutation reintroduced from outside China (*2*). Other details of the outbreak have been previously described (*3–5*). It is ideal to imitate a generic model of initial containment for countries other than China following the emergence and exportation of SARS-CoV-2 ancestral strain, as few adaptive mutations had been acquired and the herd immunity was negligible (no available vaccine and few prior SARS-CoV-2 infections) during the outbreak. The timing gap between the initial and the Xinfadi Wholesale Market outbreaks also allowed Beijing to expand its SARS-CoV-2 molecular testing capacity (with an initial testing capacity of 100,000 tests per day ramped up to 500,000 tests per day by July 7, 2020), permitting mass testing of the population at risk.

We first analyzed the highly detailed line-list data of the outbreak that had been extracted from the

Notifiable Infectious Disease Reporting System and the Epidemiological Investigation Information System of the People's Republic of China to characterize the epidemiological patterns of the outbreak. We then developed a fully stochastic, spatially structured agent-based model to reconstruct the containment effort and recover the epidemiologic patterns observed in the epidemiological data. The model structure, detailed in the Supplementary Material and Supplementary Tables S1–S5 (available in https://weekly.chinacdc.cn/), was well informed by high-resolution population mobility data, allowing us to explicitly model the targeted testing and intervention programme at high spatial resolution. Lastly, we created eight possible intervention scenarios (Levels 1–8, Table 1) by progressively layering additional NPIs on top of the prior scenario, to dissect the relative contribution of each intervention individually to the overall containment of the Xinfadi outbreak.

We ran 500 simulations with each scenario capturing the stochasticity of the transmission process. For each simulation, the following summary statistics were calculated to quantify the impact of each intervention individually: 1) the overall effective reproduction number (R_{eff}), defined as the average of the individual reproduction number of each individual infected after the implementation of NPIs; 2) the total number of infections (N) before July 10, 2020 (the end date of the Xinfadi outbreak); and 3) the proportion of undetected infections. The details of each NPI in

TABLE 1. Hypothetical intervention parameters of each NPI in different simulation scenarios.

NPI	Level 1	Level 2	Level 3	Level 4	Level 5	Level 6	Level 7	Level 8
Symptom surveillance								
Percentage of detected symptomatic infections (%)	66.7	66.7	66.7	66.7	66.7	66.7	66.7	66.7
Mask wearing								
Percentage of population wearing masks in the workplace (%)	–	20	20	20	20	20	20	20
Percentage of population wearing masks in the community (%)	–	50	50	50	50	50	50	50
Closure of the Xinfadi Wholesale Market								
Date of closure	–	–	2020-06-13	2020-06-13	2020-06-13	2020-06-13	2020-06-13	2020-06-13
Quarantine of key population								
Workers at the Xinfadi Wholesale Market	–	–	–	Centralized	Centralized	Centralized	Centralized	Centralized
Visitors to the Xinfadi Wholesale Market	–	–	–	Home	Home	Home	Home	Home
Residents around the Xinfadi Wholesale Market	–	–	–	Lockdown	Lockdown	Lockdown	Lockdown	Lockdown
Contact tracing								
Percentage of traced household contact (%)	–	–	–	–	100	100	100	100
Percentage of traced work contact (%)	–	–	–	–	100	100	100	100
Percentage of traced community contact (%)	–	–	–	–	70	70	70	70
Residential community lockdown								
Duration of lockdown after the identification of the last case (days)	–	–	–	–	–	14	14	14
Mobility restrictions*								
Percentage of mobility reductions in high-risk region (%)	–	–	–	–	–	–	70	70
Percentage of mobility reductions in moderate-risk region (%)	–	–	–	–	–	–	50	50
Percentage of mobility reductions in low-risk region (%)	–	–	–	–	–	–	20	20
Mass testing								
Rounds of RT-PCR testing	–	–	–	–	–	–	–	3

Note: "–" means not applicable.

Abbreviation: NPI=non-pharmaceutical intervention; RT-PCR=reverse transcription-polymerase chain reaction.

* The intervention parameters of mobility restrictions are defined as percentages of reductions in population flows between different risk regions during the Xinfadi outbreak, detailed in the Supplementary Table S5 (available in https://weekly.chinacdc.cn/).

response to the Xinfadi outbreak were described in the Supplementary Materials. The model was coded in Python (version 3.10.4, Python Software Foundation, Fredericksburg, VA, US). The statistical analyses and visualization were performed using R (version 4.0.2, R Foundation, Vienna, Austria).

A total of 368 SARS-CoV-2 infections were reported during the Xinfadi outbreak, including 335 (91.03%) confirmed cases and 33 (8.97%) asymptomatic infections (Figure 1A). Most of the infections were clustered in or around Huaxiang Street, where the Xinfadi Wholesale Market was located (Figure 1B), and were aged between 20 and 59 years (Figure 1C). Simulations closely imitate the real world. We present one realization of the temporal distributions of the reported infections (Figure 1D). Similar to the observed distribution in Figure 1A, a total of 355 infections were detected in the simulated outbreak, of which 18.87% were asymptomatic infections and 81.13% were confirmed cases. Figure 1E–F show the spatial distribution and age profile of the infections aggregating from the results of 500 simulated outbreaks. Both the spatial patterns and age distributions were similar to the real-world observations in Figure 1B–C, with most of the infections detected around the Xinfadi Wholesale Market and in the working age population.

To quantify the relative contribution of each individual NPI to outbreak containment, we consecutively added each intervention to the unmitigated chains of transmission. The estimated effective reproduction numbers (R_{eff}) and total number of infections (N) are reported in Figure 2A and Figure 2B. We found heterogeneity across simulations even under the same intervention intensity, reflecting the intrinsic stochasticity of SARS-CoV-2 transmission. We found that the outbreak could not be contained with only symptom surveillance (Level 1) due to the pre-symptomatic and asymptomatic transmission of SARS-CoV-2, with a median R_{eff} = 2.05 and a median N=13,421, respectively. Layering mask wearing (Level 2) and closure of Xinfadi Wholesale Market (Level 3) did not lead to significant improvement, with all simulations having effective reproduction numbers larger than 1.8, well above the epidemic threshold. Quarantine of the key populations (Level 4) could remove the potential infections from the susceptible population at the early phase of viral

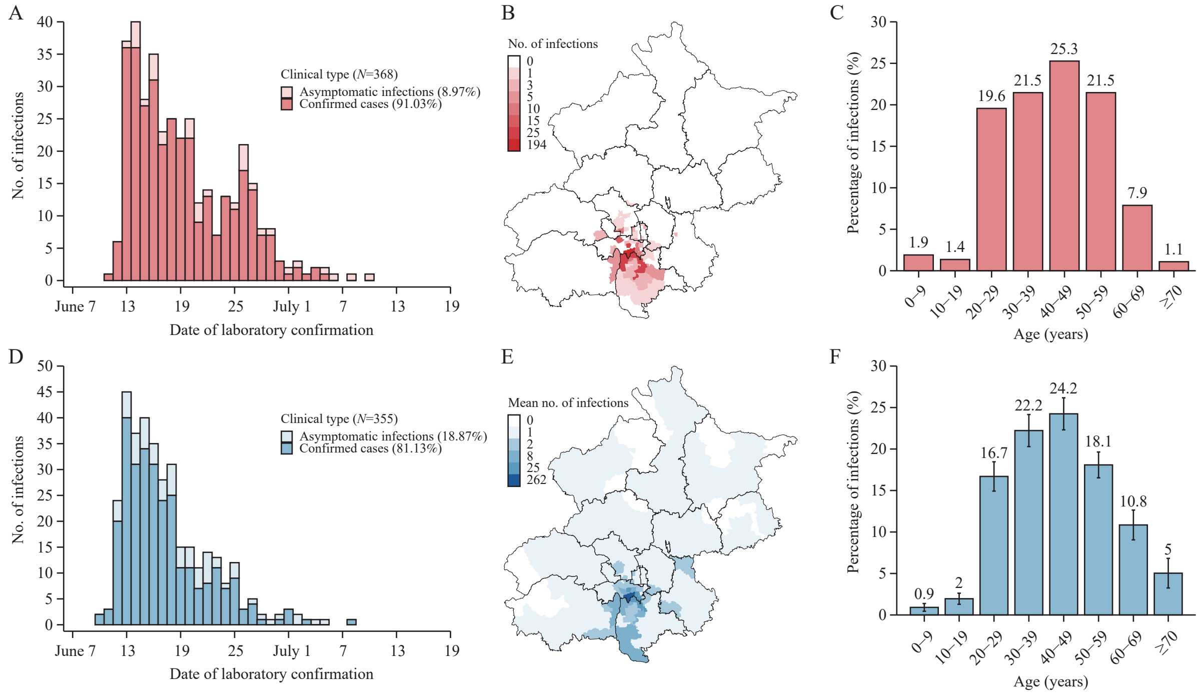

FIGURE 1. Observed and simulated epidemiologic patterns during the Xinfadi outbreak. (A) Observed temporal distribution of SARS-CoV-2 infections stratified by clinical type. (B) Observed spatial distribution of SARS-CoV-2 infections. (C) Observed age distribution of SARS-CoV-2 infections. (D) Time series of SARS-CoV-2 infections stratified by clinical type based on one simulated outbreak. (E) Spatial distribution of SARS-CoV-2 infections estimated based on 500 simulations. (F) Age distribution of SARS-CoV-2 infections estimated based on 500 simulations.

Abbreviation: SARS-CoV-2=severe acute respiratory syndrome coronavirus 2.

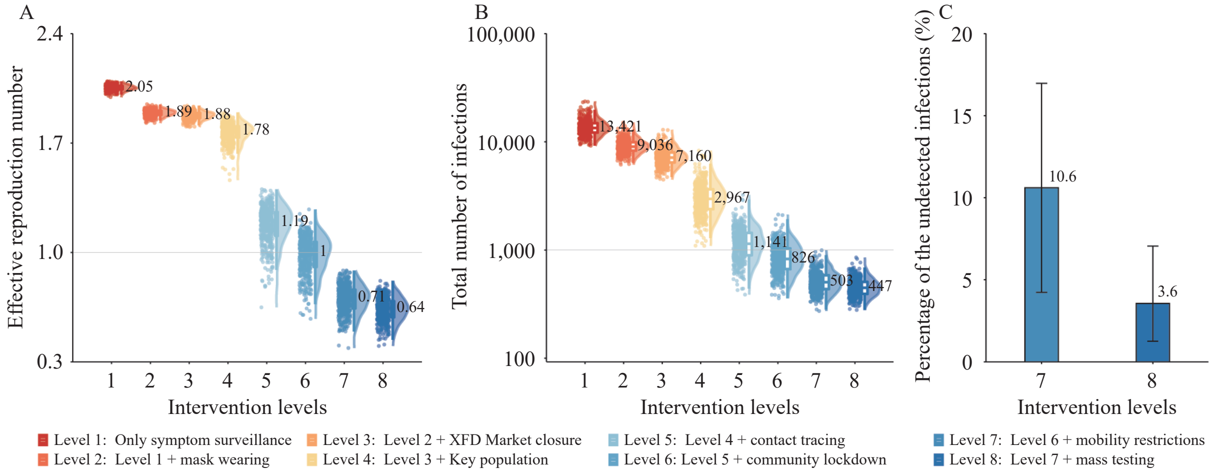

FIGURE 2. The impact of each NPI. (A) Effective reproduction numbers under different intervention scenarios. (B) Number of infections under different intervention scenarios. (C) Proportion of undetected infections.
Note: The bars represent the median of 500 simulations, and the lines give the range of the 2.5 and 97.5 quantiles.
Abbreviation: NPI=non-pharmaceutical intervention, XFD Market=Xinfadi Wholesale Market.

shedding, thus effectively reducing the number of infections (median N=2,967), but the further transmission could not be suppressed (median R_{eff} = 1.78). Contact tracing (Level 5), in contrast, could significantly reduce further transmission, leading to fewer infections (median N=1,141) and lower effective reproduction numbers (median R_{eff} = 1.19), but for most simulations, the estimated R_{eff} was still above the epidemic threshold, indicating that containment could not be achieved through Level 5 intervention intensity. With lockdown of infected individuals' residential communities (Level 6), the median R_{eff} hovered around the epidemic threshold of 1, resulting in highly stochastic outcomes with the probability of achieving containment at 50%. Implementing targeted population mobility restrictions (Level 7) would achieve the goal of containment, with the estimated R_{eff} ranging from 0.39 to 0.89 and the number of infections less than 1,000 for all simulations. Although the outbreak could be suppressed with Level 7 intervention intensity, additional mass testing at the street/town level was adopted during the Xinfadi outbreak, which could further reduce the effective reproduction number and the number of infections, with a median R_{eff} = 0.64 and a median N=447, leading to faster clearance and fewer infections. Furthermore, we found that approximately 10.6% of the infections were undetected in the absence of mass testing (Level 7), while the number of undetected infections fell to 3.6% after the implementation of mass testing (Level 8), indicating that the outbreak could be contained earlier through mass testing, with more infections being detected and isolated, and thus the onward transmission could be truncated (Figure 2C).

DISCUSSION

In this study, we demonstrated through both empirical data and modeling analysis that a multilayer deployment of targeted NPIs could easily contain outbreaks caused by the SARS-CoV-2 ancestral strain. We found that robust implementation of symptom surveillance and high-risk population screening served as sentinels to discover cryptic community transmission in the early stage of the outbreak. Effective contact tracing combined with case isolation and close contact quarantine has been shown to substantially reduce transmission, highlighting the importance of training and maintaining epidemiologic teams with field experience. Targeted community lockdown and rapid turnaround of molecular testing for the confined population could further limit undetected infections missed by contact tracing, as the transmission of SARS-CoV-2 demonstrates clear spatial clustering. It is more cost-effective than population-wide lockdowns, with fewer people being affected. Temporal reductions in mobility (rather than blanket lockdowns) in and out of regions with high infection risk could slow down the spatial dissemination of the outbreak. If conditions permit, population-wide mass testing could further improve the speed of outbreak containment. These evidences carried critical policy implications for the ongoing COVID-19 pandemic and other epidemics caused by newly emerged pathogens.

Currently, the adaptive evolution of SARS-CoV-2 continues with no sign of slowing down, with multiple sublineages of SARS-CoV-2 Omicron emerging continuously and causing recurring Omicron waves despite high levels of population immunity achieved by vaccination and natural infection. In addition, unmitigated spreading could also lead to spillover into other animal reservoirs (*6*), leaving pathogen eradication impossible to achieve. In contrast, at the beginning of the pandemic, even with negligible population immunity (i.e., no effective vaccine available), due to the limited transmissibility of the ancestral strain (R_0=2.5) (*7*), multiple regions across all socioeconomic statuses successfully achieved temporal suppression of SARS-CoV-2 in the early stage of the pandemic through the implementation of NPIs. In retrospect, had the virus been successfully contained in the early stage of the pandemic, a great deal of the global morbidity, mortality and tremendous socioeconomic costs could have been avoided.

This study was subject to some limitations. First, it suffers from the uncertainty of epidemiological parameters from previous estimates, such as the distribution of the generation interval and the age-specific asymptomatic rates. Second, the temporal span of our simulations is limited. Finally, we cannot simulate all the NPIs during the Xinfadi outbreak, such as the population screening based on the positive environmental samples.

Our study clearly demonstrated that the containment of the SARS-CoV-2 ancestral strain would have been achievable through NPIs once a reliable and scalable diagnostic test became available. More broadly, the critical opportunity window for containing a newly emerged pathogen is in the very early stage of the pandemic, before the pathogen has the opportunity to evolve and adapt in the human population with greatly enhanced transmissibility and immune evasion properties, if all countries decide to pursue such strategies collectively. Furthermore, sustaining SARS-CoV-2 local containment at the early stage of the pandemic could buy some time to achieve high immunization coverage as well as stockpile effective antiviral drugs, potentially ensuring a smooth transition to mitigation strategies while minimizing the overall disease burden.

Conflicts of interest: The findings and conclusions in this study are those of the authors and do not necessarily represent the official position of the funding agencies, the National Institutes of Health, or the U.S. Department of Health and Human Services.

Funding: Supported by grants from the Key Program of the National Natural Science Foundation of China (82130093) and Shanghai Municipal Science and Technology Major Project (ZD2021CY001).

doi: 10.46234/ccdcw2023.020

[#] Corresponding authors: Hongjie Yu, yhj@fudan.edu.cn; Quanyi Wang, wangqy@bjcdc.org.

---

[1] School of Public Health, Fudan University, Key Laboratory of Public Health Safety, Ministry of Education, Shanghai Municipality, China; [2] Division of International Epidemiology and Population Studies, Fogarty International Center, National Institutes of Health, Bethesda, MD, USA; [3] Beijing Center for Disease Prevention and Control, Beijing Municipality, China; [4] Shanghai Institute of Infectious Disease and Biosecurity, Fudan University, Shanghai Municipality, China.
[&] Joint first authors.

Submitted: November 13, 2022; Accepted: January 09, 2023

REFERENCES

1. World Health Organization. WHO coronavirus (COVID-19) dashboard. 2022. https://covid19.who.int/. [2022-8-6].
2. Pang XH, Ren LL, Wu SS, Ma WT, Yang J, Di L, et al. Cold-chain food contamination as the possible origin of COVID-19 resurgence in Beijing. Natl Sci Rev 2020;7(12):1861 – 4. http://dx.doi.org/10.1093/nsr/nwaa264.
3. Wang XL, Lin X, Yang P, Wu ZY, Li G, McGoogan JM, et al. Coronavirus disease 2019 outbreak in Beijing's Xinfadi Market, China: a modeling study to inform future resurgence response. Infect Dis Poverty 2021;10(1):62. http://dx.doi.org/10.1186/s40249-021-00843-2.
4. Wu ZY, Wang QY, Zhao J, Yang P, McGoogan JM, Feng ZJ, et al. Time course of a second outbreak of COVID-19 in Beijing, China, June-July 2020. JAMA 2020;324(14):1458 – 9. http://dx.doi.org/10.1001/jama.2020.15894.
5. Wenjie Tan, Peihua Niu, Xiang Zhao, Yang Pan, Yong Zhang, Lijuan Chen, et al. Reemergent Cases of COVID-19 — Xinfadi Wholesale Market, Beijing Municipality, China, June 11, 2020. China CDC Weekly 2020;2(27):502 – 4. http://dx.doi.org/10.46234/ccdcw2020.132.
6. Yen HL, Sit THC, Brackman CJ, Chuk SSY, Gu HG, Tam KWS, et al. Transmission of SARS-CoV-2 delta variant (AY. 127) from pet hamsters to humans, leading to onward human-to-human transmission: a case study. Lancet 2022;399(10329):1070 – 8. http://dx.doi.org/10.1016/s0140-6736(22)00326-9.
7. Imai N, Cori A, Dorigatti I, Baguelin M, Donnelly CA, Riley S, et al. Report 3: transmissibility of 2019-nCoV. Imperial College London; 2020. http://dx.doi.org/10.25561/77148.

SUPPLEMENTARY MATERIAL

Initial Infections

We defined the 169 infected workers at the Xinfadi Wholesale Market as initial infections. For each initial infection *i,* the time of infection t_i^{inf} was either generated by subtracting a randomly sampled incubation period from the reported time of symptom onset (for a symptomatic case) or by subtracting a randomly sampled time delay from infection to diagnosis from the time of laboratory confirmation (for an asymptomatic case). The sampled time of infection was constrained within the exposure window identified by epidemiological investigation.

SARS-CoV-2 Transmission as Branching Processes

We first generated each initial infection *i*'s reproduction number R_i (number of secondary infections caused by *i*). For unmitigated transmission, we assumed that R_i followed a negative binomial distribution $NB(R_0, k)$, where R_0 is the basic reproduction number representing the population average of R_i and k is the dispersion parameter capturing the heterogeneity of SARS-CoV-2 transmission. For each secondary infection $j \in \{R_i\}$, the infection time t_j^{inf} is given by $t_j^{inf} = t_i^{inf} + \tau_{ij}$, where τ_{ij} denotes the generation interval of transmission from *i* to *j*, drawn from a generation interval distribution $P_{GI}(\tau)$. Then, we hypothesized that the proportion of asymptomatic infection Φ_{asymp} decreased with age. For a symptomatic case *j*, we assigned his or her symptom onset date t_j^{sym} by drawing from the incubation period distribution $P_{incu}(\tau)$. The parameters reflecting the transmission dynamics and the natural history of COVID-19 are summarized in Supplementary Table S1.

Population Structure Reflecting Demographics, Transmission Setting, and Activity

When transmission between primary infection *i* and secondary infection *j* occurred, we first generated the transmission setting based on the predefined probability that the transmission event occurred at home ($\varnothing_{hh}$), in the workplace ($\varnothing_{wk}$) or in the community ($\varnothing_{cm}$). The hypothesized conditional probabilities are summarized in Supplementary Table S2, where we assumed that i) all service workers worked in the community and ii) all general workers did not work on holidays or weekends. For any transmission event occurring in the community, the activities of primary infection *i* (Act_i) and secondary infection *j* (Act_j) at the time of transmission were assigned based on their occupation. Service workers who worked in the community could be assigned either work or social activity, with probabilities of ϕ_{cm}^{wk}=0.6 and ϕ_{cm}^{soc}=0.4, respectively. For general workers and nonworkers, we assumed that only social activity was possible in the community (i.e., $\phi_{cm}^{wk} = 0$).

The age of secondary infection *j* was then assigned based on transmission settings, age-stratified contact matrices and age-specific susceptibility to SARS-CoV-2 infection. We defined the age-specific contact matrices [derived from a prior study (*6*) and contact tracing data] as C^{hh}, C^{wk}, and C^{cm} for household, workplace, and community contact, respectively. Each cell of the matrix (c_{mk}^T) represents the average number of contacts in age group k of an individual in age group m in a given setting T. For any contact in age group k, whether he or she became infected depended on the age-specific susceptibility to SARS-CoV-2 infection $risk_k^{inf}$ (derived from contact tracing data, Supplementary Table S3). Therefore, the probability that *j* is in age group a_j is given by

SUPPLEMENTARY TABLE S1. Parameters reflecting the transmission dynamics and the natural history of COVID-19.

Parameter	Description	Value
R_0	Basic reproduction number	2.5 (*1*)
k	Dispersion parameter capturing the heterogeneity of SARS-CoV-2 transmission	0.43 (*2*)
$P_{GI}(\tau)$	Distribution of generation interval	Gamma distribution (shape=13.86, rate=2.07) (*3*)
Φ_{asymp}	Age-specific asymptomatic rate	46.7% for 0–18 years 32.1% for 19–59 years 19.7% for 60+ years (*4*)
$P_{incu}(\tau)$	Distribution of the incubation period	Gamma distribution (derived from the epidemiological data) (shape=2.25, rate=0.39)

Abbreviation: COVID-19=coronavirus disease 2019; SARS-CoV-2=severe acute respiratory syndrome coronavirus 2.

SUPPLEMENTARY TABLE S2. Hypothetical probability that the transmission event occurred at home, in the workplace or in the community.

Condition		**Hypothetical probability**		
Occupation of primary infection *i* (O_i)	**Time of transmission (t_j^{inf})**	$\varnothing_{hh}$	$\varnothing_{wk}$	$\varnothing_{cm}$
$hh\_suscept_i^{*} = 0$				
General worker	Workday	0	0.6	0.4
	Holiday/weekend	0	0	1
Service worker	–	0	0	1
Nonworker	–	0	0	1
$hh\_suscept_i^{*} > 0$				
General worker	Workday	0.5	0.3	0.2
	Holiday/weekend	0.7	0	0.3
Service worker	–	0.5	0	0.5
Nonworker	–	0.7	0	0.3

Note: “–” means not applicable.

* $hh\_suscept_i$ denotes the number of susceptible individuals in primary infection *i*’s home at the time of transmission.

SUPPLEMENTARY TABLE S3. Age-specific susceptibility to SARS-CoV-2 infection.

Age group (*k*)	**Relative risk $\left(risk_k^{inf}\right)$**
0–14 years	0.25
15–29 years	0.79
30–49 years	1
50–64 years	1.13
65+ years	1.32

$$P^{T}_{a_j|a_i} = \frac{c^{T}_{a_i a_j} risk^{inf}_{a_j}}{\sum_k C^{T}_{a_i k} risk^{inf}_{k}}$$

where a_i is the age group of primary infection *i*. The sex of secondary infections was generated completely at random, except for individuals infected in the workplace aged 55–59 years (who were males because females retire from work at 55 years of age).

To assign secondary infection *j*’s occupation, we first determined whether he or she was a worker (i.e., 18–59 years for a male; 18–54 years for a female) according to his or her age and sex. We then divided workers into general workers (GW) and service workers (SW). Service workers were further divided into workers at the Xinfadi Wholesale Market (XFD-SW) and other service workers (Other-SW). For any infected worker *j*, we stochastically determined his or her specific occupation based on the predefined probability that the secondary infection *j* worked as a general worker (ψ_j^{GW}), a service worker at the Xinfadi Wholesale Market (ψ_j^{XFD-SW}) or a service worker in other places ($\psi_j^{Other-SW}$). The hypothetical probabilities conditional on the transmission setting (T_{ij}), activity (Act_i) and occupation (O_i) of primary infection *i* are summarized in Supplementary Table S4.

Population Interaction Network Based on Spatially Resolved Mobility Patterns

To emulate the spatial dispersion of SARS-CoV-2 infections, we first constructed the spatially resolved population mobility patterns in Beijing on the basis of the mobility data and then developed a network interaction model based on the constructed mobility patterns to stochastically assign the residential locations of each person with an infection, the workplace of each worker and the location for social activity if the transmission occurred through social contact. Details are described below.

Mobility data: The aggregated mobile phone signaling data were provided by China Unicom, one of the leading mobile phone service providers in China. The data were aggregated as origin-destination matrices (O-D matrices)

SUPPLEMENTARY TABLE S4. Hypothetical probability that the secondary infection j worked as a general worker, a service worker at the Xinfadi Wholesale Market or a service worker in other places.

Condition		Hypothetical probability*		
T_{ij}	Act_i	ψ_j^{GW}	$\psi_j^{XFD\text{-}SW}$	$\psi_j^{Other\text{-}SW}$
O_i=GW				
At home	–	0.903	0	0.097
In the workplace	–	1	0	0
In the community	Social activity	0.903	0	0.097
O_i=XFD-SW				
At home	–	0.72	0.2	0.08
In the community	Work	0.4	0.2	0.4
In the community	Social activity	0.72	0.2	0.08
O_i=Other-SW				
At home	–	0.903	0	0.097
In the community	Work	0.8	0	0.2
In the community	Social activity	0.903	0	0.097
O_i=Nonworker				
At home	–	0.903	0	0.097
In the community	Social activity	0.903	0	0.097

Note: "–" means not applicable.

Abbreviation: GW=general worker; XFD-SW=service worker at the Xinfadi Market; Other-SW=service worker in other places.

* The probabilities are hypothesized based on epidemiological investigations of the outbreak and the demographical structures in Beijing (7).

stratified by age and sex group, where the rows and the columns represent the origin and destination streets/towns, respectively. Each cell of the matrix represents the total number of trips of the subscribers from the origin to the destination in a given age and sex group during a certain period of time (in hours).

Spatially resolved mobility patterns in Beijing: By aggregating the mobility data, we obtained the average number of trips from the origin location O to the destination location D at time t in a given age and sex group on workday $n_{O\to D}^{wkd}(t|\,age,sex)$ and on holiday $n_{O\to D}^{hld}(t|\,age,sex)$, respectively. Assuming that the working-age population goes to work during morning rush hours (i.e., between 6:00 a.m. and 10:00 a.m. on workdays), we estimated the average daily trips from location O to location D for work ($n_{O\to D}^{work}$) as $n_{O\to D}^{work}=\sum_{t=6}^{10}n_{O\to D}^{wkd}(t|\,wk\_age)$, where wk_age refers to working age groups (i.e., 18–59 years for males and 18–54 years for females). Since service workers provide social services to the general population, we assumed that their spatial mobility patterns for work were in accordance with and accounted for 10% of the population flows on holiday morning rush hours. Therefore, the average number of daily trips of the service workers from O to D for work $n_{O\to D}^{sw}$ is given by $n_{O\to D}^{sw}=0.1\times\sum_{t=6}^{10}n_{O\to D}^{hld}(t|\,wk\_age)$, and that of the general workers $n_{O\to D}^{gw}$ can be derived as $n_{O\to D}^{gw}=n_{O\to D}^{work}-n_{O\to D}^{sw}$. Trips at other times or of other age groups were considered as social activities. Assuming that those who live in location D and work at location O would travel from D to O in the morning and back from O to D in the evening, the average daily trips from O to D for social activities are given as $n_{O\to D}^{soc\_wkd}=\sum_t n_{O\to D}^{wkd}(t|\,all)-n_{O\to D}^{work}-n_{D\to O}^{work}$ (on workday) and $n_{O\to D}^{soc\_hld}=\sum_t n_{O\to D}^{hld}(t|\,all)-n_{O\to D}^{sw}-n_{D\to O}^{sw}$ (on holiday), where all refers to all age and sex groups.

Then, the interaction matrices reflecting the population mobility patterns in Beijing in the absence of non-pharmaceutical interventions were constructed based on the aggregated data before the Xinfadi outbreak (from June 1 to June 12, 2020), with each row of the matrices representing the origin street/town (i.e., residential location) and each column representing the destination street/town (i.e., location for work or social activity). Specifically, the interaction matrices for work are defined as I^{gw} (for general workers) and I^{sw} (for service workers), of which each cell represents the probability of working at location D for an individual living in location O, given as $I_{O\to D}^{gw}=\frac{n_{O\to D}^{gw}}{\sum_K n_{O\to K}^{gw}}$ and $I_{O\to D}^{sw}=\frac{n_{O\to D}^{sw}}{\sum_K n_{O\to K}^{sw}}$. Similarly, the interaction matrices reflecting the social mobility patterns on workday (I^{soc_wkd})

and on holiday (I^{soc_hld}) are constructed as $I^{soc\_wkd}_{O\to D} = \frac{n^{soc\_wkd}_{O\to D}}{\sum_K n^{soc\_wkd}_{O\to K}}$ and $I^{soc\_hld}_{O\to D} = \frac{n^{soc\_hld}_{O\to D}}{\sum_K n^{soc\_hld}_{O\to K}}$, respectively.

Network interaction model: Locations of secondary infections were stochastically allocated using a spatially structured network interaction model based on the constructed mobility patterns. We first created a unique block identification number *blk_id* for each residential block and a unique household identification number *hh_id* for each family, where residents of a block share the same *blk_id* and members of a household share the same *hh_id*.

Household transmission: For any transmission occurred at home,the residential location and household size of the secondary infection j were the same as those of the primary infector i, i.e., $loc\_resid_j = loc\_resid_i$, $blk\_id_j = blk\_id_i$, $hh\_id_j = hh\_id_i$, $hh\_size_j = hh\_size_i$. The workplace of j (loc_wk_j) is then chosen based on the mobility patterns, given as $P_{(loc\_wk_j = D)} = I^{gw}_{loc\_resid_j \to D}$ (if j is a general worker) or $P_{(loc\_wk_j = D)} = I^{sw}_{loc\_resid_j \to D}$ (if j is a service worker), where $P_{(loc\_wk_j = D)}$ indicates the probability that j worked at location D.

Workplace transmission: If a transmission event occurred in the workplace, we have $loc\_wk_j = loc\_wk_i$. The residential street/town of the secondary infection j was then allocated according to the mobility patterns, given as $P_{(loc\_resid_j = O)} = I^{gw}_{O\to loc\_wk_j}$. We further randomly chose a *blk_id* and a *hh_id* for j within his or her residential street/town and stochastically generated j's household size based on the age-specific household size distribution (*6*).

Community transmission: For any transmission that occurred in the community, we first allocated a transmission location ($loc^{trans}_{i\to j}$). If i infected j through work contact (i.e., $\mathrm{Act}_i = work$), we have $loc^{trans}_{i\to j} = loc\_wk_i$. Otherwise, if i infected j through social contact (i.e., $\mathrm{Act}_i = social$), $loc^{trans}_{i\to j}$ is stochastically generated following the probabilities given as $P_{(loc^{trans}_{i\to j} = D)} = I^{soc\_wkd}_{loc\_resid_i \to D}$ (on a workday) or $P_{(loc^{trans}_{i\to j} = D)} = I^{soc\_hld}_{loc\_resid_i \to D}$ (on a holiday). Then, j's residential street/town and workplace are generated according to Act_j and $loc^{trans}_{i\to j}$: (i) if j was infected through work contact (i.e., $\mathrm{Act}_j = work$), we have $loc\_wk_j = loc^{trans}_{i\to j}$. The residential location of j is randomly generated following the probability $P_{(loc\_resid_j = O)} = I^{sw}_{O\to loc\_wk_j}$. (ii) If j was infected through social contact (i.e., $\mathrm{Act}_j = social$), we first randomly assigned j's residential location based on the population mobility patterns, given as $P_{(loc\_resid_j = O)} = I^{soc\_wkd}_{\mathrm{O}\to loc^{trans}_{i\to j}}$ (on workday) and $P_{(loc\_resid_j = O)} = I^{soc\_hld}_{\mathrm{O}\to loc^{trans}_{i\to j}}$ (on holiday). The workplace of j (loc_wk_j) is then chosen according to his or her occupation, given as $P_{(loc\_wk_j = D)} = I^{gw}_{loc\_resid_j \to D}$ (if j is a general worker) or $P_{(loc\_wk_j = D)} = I^{sw}_{loc\_resid_j \to D}$ (if j is a service worker). Finally, we randomly chose a *blk_id* and a *hh_id* for j within his or her residential street/town and stochastically generated j's household size based on the age-specific household size distribution (*6*).

Non-Pharmaceutical Interventions (NPIs)

Symptomatic surveillance: Initially, we assumed that 33.3% of the people with symptomatic infections (i.e., $\Phi_{hosp} = 33.3\%$) would seek medical attention after a mean time delay of 3.7 days from the onset of symptoms. After the official report of the outbreak on June 13, 2020, with enhanced symptom surveillance in the community, we assumed that more people with symptomatic infections (i.e., $\Phi_{hosp} = 66.7\%$) would seek health care consultation after a shorter time delay with a mean of 2.7 days from symptom onset. Three RT-PCR (i.e., reverse transcription polymerase chain reaction) tests for SARS-CoV-2 diagnosis were conducted on the 1st, 3rd and 7th days of isolation. The sensitivity of RT-PCR testing was assumed to vary with time, following the estimates of a prior study (*8*).

Mask wearing: We assume 20% of the population would wear masks in the workplace and 50% in the community. The protective effect of mask wearing against further transmission and infection of SARS-CoV-2 was assumed to be 9.5% and 18%, respectively (*9–10*).

Closure of the Xinfadi Wholesale Market: The Xinfadi Wholesale Market was closed on June 13, 2020.

Quarantine and testing of key populations: Workers at the Xinfadi Wholesale Market were quarantined in centralized facilities for at least 14 days. Periodic RT-PCR testing was conducted on the 1st, 4th, 7th, and 14th days of quarantine and the 2nd and 7th days after discharge. Visitors who had been to the Xinfadi Wholesale Market between May 30 and June 12, 2020, were asked to stay at home for 14 days. RT-PCR testing was performed on the 1st, 7th and 14th days of home quarantine. Residents living around the Xinfadi Wholesale Market were confined to their living communities from June 13, 2020, until no new infections were reported for 14 consecutive days. Mass testing was implemented every seven days during the lockdown period.

Contact tracing: Close contact was defined as a person who interacted with a confirmed case from 4 days before to 14 days after illness onset or with an asymptomatic carrier from 4 days before to 14 days after collection of the first positive sample. We assumed that all household contacts were immediately quarantined, while all work contacts and 70% of the community contacts quarantined with a mean time delay of 3 days. Centralized quarantine at designated facilities for at least 14 days was required for all close contacts, with periodic RT-PCR testing on the 1st, 4th, 7th, and 14th days of quarantine and the 2nd and 7th days after discharge.

Residential community lockdown: Since June 13, 2020, residential communities with detected infections have been on lockdown at the block level until 14 days after the identification of the last case, with stay-at-home orders for all residents other than essential workers.

Mobility restrictions: During the Xinfadi outbreak, the street/town was upgraded to moderate risk once it had reported more than one infection and then upgraded to high risk when more than 5 infections were reported, while other regions, with or without one detected infection, remained low-risk areas. We quantified the reduction in population flows and constructed the origin-destination mobility matrix between different risk regions based on mobility data (Supplementary Table S5).

SUPPLEMENTARY TABLE S5. The hypothetical origin-destination mobility matrix depending on risk levels.

Risk level of the origin street/town	Risk level of the destination street/town			Mobility within one street/town
	High	Moderate	Low	
High	0	0.1	0.3	0.3
Moderate	0.1	0.3	0.5	0.6
Low	0.3	0.5	0.8	0.9

Note: The risk level refers to the real-time risk level of the street/town at the time of transmission. The value in each cell of the matrix refers to the average travel probability per person after the Xinfadi outbreak, given the risk level of the origin and destination regions.

Mass testing: Three rounds of RT-PCR testing were required for all residents living in streets/towns with detected infections, with each round of mass testing being completed within 3–4 days. The interval between each round of testing was usually 7 days.

REFERENCES

1. Imai N, Cori A, Dorigatti I, Baguelin M, Donnelly CA, Riley S, et al. Report 3: transmissibility of 2019-nCoV. Imperial College London; 2020. http://dx.doi.org/10.25561/77148.
2. Adam DC, Wu P, Wong JY, Lau EHY, Tsang TK, Cauchemez S, et al. Clustering and superspreading potential of SARS-CoV-2 infections in Hong Kong. Nat Med 2020;26(11):1714 – 9. http://dx.doi.org/10.1038/s41591-020-1092-0.
3. Zhao S, Tang B, Musa SS, Ma SJ, Zhang JY, Zeng MY, et al. Estimating the generation interval and inferring the latent period of COVID-19 from the contact tracing data. Epidemics 2021;36:100482. http://dx.doi.org/10.1016/j.epidem.2021.100482.
4. Sah P, Fitzpatrick MC, Zimmer CF, Abdollahi E, Juden-Kelly L, Moghadas SM, et al. Asymptomatic SARS-CoV-2 infection: a systematic review and meta-analysis. Proc Natl Acad Sci USA 2021;118(34):e2109229118. http://dx.doi.org/10.1073/pnas.2109229118.
5. Zhang JJ, Klepac P, Read JM, Rosello A, Wang XL, Lai SJ, et al. Patterns of human social contact and contact with animals in Shanghai, China. Sci Rep 2019;9(1):15141. http://dx.doi.org/10.1038/s41598-019-51609-8.
6. Beijing Municipal Bureau of Statistics, Survey Office of the National Bureau of Statistics in Beijing. Annual statistics of population and employment in Beijing in 2021. 2020. http://tjj.beijing.gov.cn/tjsj_31433/tjbmfbjh/ndtjzl_31437/2021ndtjzl/202012/t20201231_2191210.html. [2022-8-6]. (In Chinese).
7. Kucirka LM, Lauer SA, Laeyendecker O, Boon D, Lessler J. Variation in false-negative rate of reverse transcriptase polymerase chain reaction-based SARS-CoV-2 tests by time since exposure. Ann Intern Med 2020;173(4):262 – 7. http://dx.doi.org/10.7326/m20-1495.
8. Bundgaard H, Bundgaard JS, Raaschou-Pedersen DET, von Buchwald C, Todsen T, Norsk JB, et al. Effectiveness of adding a mask recommendation to other public health measures to prevent SARS-CoV-2 infection in Danish mask wearers: a randomized controlled trial. Ann Intern Med 2021;174(3):335 – 43. http://dx.doi.org/10.7326/m20-6817.
9. Leech G, Rogers-Smith C, Sandbrink JB, Snodin B, Zinkov R, Rader B, et al. Mass mask-wearing notably reduces COVID-19 transmission. medRxiv 2021. http://dx.doi.org/10.1101/2021.06.16.21258817.

Methods and Applications

Estimating Changes in Contact Patterns in China Over the First Year of the COVID-19 Pandemic: Implications for SARS-CoV-2 Spread — Four Cities, China, 2020

Yuxia Liang[1]; Cheng Peng[1]; Qian You[1]; Maria Litvinova[2]; Marco Ajelli[2]; Juanjuan Zhang[1,#]; Hongjie Yu[1,3,#]

ABSTRACT

Introduction: Previous studies have demonstrated significant changes in social contacts during the first-wave coronavirus disease 2019 (COVID-19) in Chinese mainland. The purpose of this study was to quantify the time-varying contact patterns by age in Chinese mainland in 2020 and evaluate their impact on the transmission of severe acute respiratory syndrome coronavirus 2 (SARS-CoV-2).

Methods: Diary-based contact surveys were performed for four periods: baseline (prior to 2020), outbreak (February 2020), post-lockdown (March–May 2020), and post-epidemic (September–November 2020). We built a Susceptible-Infected-Recovered (SIR) model to evaluate the effect of reducing contacts on transmission.

Results: During the post-epidemic period, daily contacts resumed to 26.7%, 14.8%, 46.8%, and 44.2% of the pre-COVID levels in Wuhan, Shanghai, Shenzhen, and Changsha, respectively. This suggests a moderate risk of resurgence in Changsha, Shenzhen, and Wuhan, and a low risk in Shanghai. School closure alone was not enough to interrupt transmission of SARS-CoV-2 Omicron BA.5, but with the addition of a 75% reduction of contacts at the workplace, it could lead to a 16.8% reduction of the attack rate. To control an outbreak, concerted strategies that target schools, workplaces, and community contacts are needed.

Discussion: Monitoring contact patterns by age is key to quantifying the risk of COVID-19 outbreaks and evaluating the impact of intervention strategies.

After the first wave of coronavirus disease 2019 (COVID-19) in China in early 2020, social distancing policies were gradually relaxed. A series of studies were conducted to quantify the changes in contact patterns under different interventions, whose intensity and type varied over time, and to estimate their impact on the epidemic spread (*1*–*3*). Previous studies have shown a dramatic decrease in the number of social interactions in China during the early phase of the pandemic (*1*). This was followed by a moderate increase in social contacts after strict non-pharmaceutical interventions (NPIs) were relaxed from March to May 2020 (*2*–*3*). As of the fourth quarter of 2020, almost all schools and workplaces had been opened (*4*–*5*), and daily life had gradually resumed to a normal status. It is still unknown to what extent social interactions had resumed by the end of 2020 and how age-specific contact patterns had affected severe acute respiratory syndrome coronavirus 2 (SARS-CoV-2) transmission in China. The purpose of this study was to estimate changes in contact patterns by age in Chinese mainland over the course of the first year of the COVID-19 pandemic. This study aimed to provide valuable information about the risk of transmission and transmission patterns by age in a post-COVID-19-intervention context.

METHODS

To estimate changes in contact patterns by age in the post-epidemic period, we conducted diary-based contact surveys in Wuhan, Shanghai, Shenzhen, and Changsha between September 16 and November 8, 2020 (Figure 1). The design of the survey (Supplementary Material, available in https://weekly.chinacdc.cn/) was similar to that of our previous work (*1*–*2*,*6*), where contact patterns during the pre-pandemic (prior to 2020), outbreak (February 2020), and post-lockdown (March to May 2020) periods were investigated (Figure 1). A contact was defined as either a two-way conversation involving three or more words in the physical presence of another person or direct physical contact (e.g., a handshake). We further divided direct interpersonal contact into three types: 1)

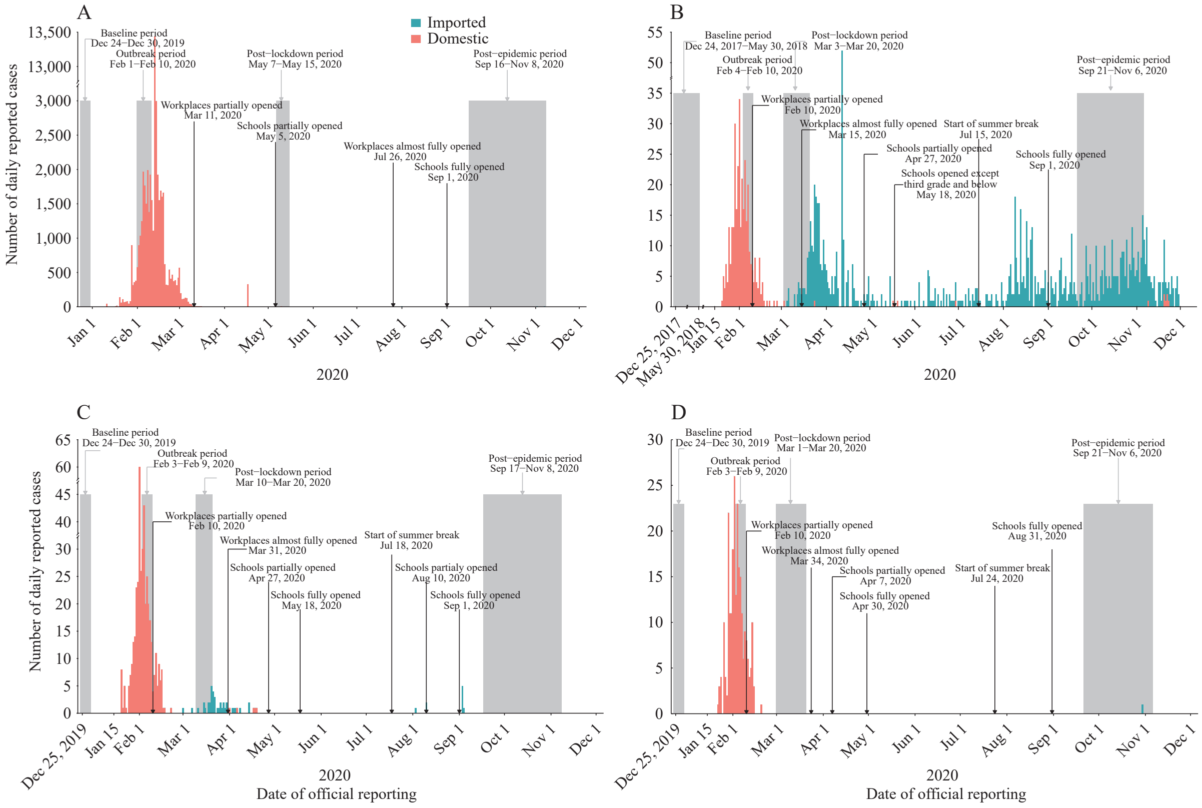

FIGURE 1. Number of reported locally transmitted (red) and imported (green) COVID-19 cases, summary of the main interventions performed over time, and timeline of the surveys in Wuhan (A), Shanghai (B), Shenzhen (C), and Changsha (D).

physical contact, 2) non-physical contact at a distance of 1 meter or less, and 3) non-physical contact at a distance of more than 1 meter. We also recorded whether the participant and contact were wearing face masks (i.e., both wore, neither wore, or one wore), and the contact environment (i.e., indoor, outdoor, or both).

We estimated contact matrices by age, dividing participants into 16 age groups (0–4 years, 5–9 years, ... , 70–74 years, and 75 years and older). We relied on data collected from this survey and three other surveys conducted during the pre-pandemic, outbreak, and post-lockdown periods to estimate contact matrices representing mixing patterns for the four cities (*1*–*2*,*6*).

We estimated the impact of daily life resumption on the potential reproduction number (*R*) of a COVID-19 outbreak by relying on the mixing patterns estimated in contact surveys. The next-generation matrix approach was used to estimate *R*. To evaluate the impact on transmission dynamics of reducing school, workplace, and community contacts, we simulated a possible outbreak of SARS-CoV-2 Omicron BA.5 or another highly transmissible variant using an ordinary differential equation Susceptible-Infectious-Removed (SIR) model (Supplementary Material, available in https://weekly.chinacdc.cn/). We used Shanghai as a case study, based on the baseline contact matrix by setting. We assumed that eliminating contacts in a certain setting while keeping the contacts in other settings the same as the baseline period would indicate closure of that setting. We designed four scenarios to estimate the effect of different social distancing strategies: 1) Baseline scenario (no interventions): workplace, school, and community contacts were at pre-COVID levels; 2) Scenario 1: no contacts at school, while all other contacts were at pre-COVID levels; 3) Scenario 2: no contacts at school and a 75% reduction of contacts at the workplace, while all other contacts were at pre-COVID levels; and 4) Scenario 3: no contacts at school, a 75% reduction of contacts at the workplace, and a 90% reduction of contacts in the community. Scenarios 2 and 3 simulated a 75% and 90% reduction of contacts in the workplace and community, respectively. During the first COVID-19 lockdown in Shanghai, we estimated a nearly 90% reduction of workplace contacts and a 95% reduction of contacts in the community (*1*). As achieving such a high level of reduction may be difficult without imposing a strict lockdown, we used more conservative estimates of a 75% and 90% reduction of workplace and community contacts, respectively.

All the analyses were performed in R (version 4.0.3, R Foundation for Statistical Computing, Vienna, Austria).

RESULTS

A total of 3,281 participants (858 from Wuhan, 832 from Shanghai, 797 from Shenzhen, and 794 from Changsha) were recruited for the post-epidemic survey, and 16,533 contacts were recorded in total. Compared with the outbreak period, the average number of contacts during the post-epidemic period significantly increased by a factor of 1.9 (*P*<0.001), 0.5 (*P*<0.001), 1.5 (*P*<0.001), and 2.0 (*P*<0.001) in Wuhan, Shanghai, Shenzhen, and Changsha, respectively (Supplementary Table S1, available in https://weekly.chinacdc.cn/). The largest resumption of contacts was observed for school-age individuals (Supplementary Figure S1, available in https://weekly.chinacdc.cn/). In Wuhan, 18.9% of contacts were non-physical contacts at a distance of at least 1 meter, 39.6% of contacts occurred with both or either the participant or the contactee wearing a face mask, and 9.6% of contacts occurred outdoors. Similar contact patterns were observed in Shanghai, Shenzhen, and Changsha (Supplementary Figure S2, available in https://weekly.chinacdc.cn/).

The pre-pandemic (baseline) contact matrices revealed the typical age-mixing patterns observed in

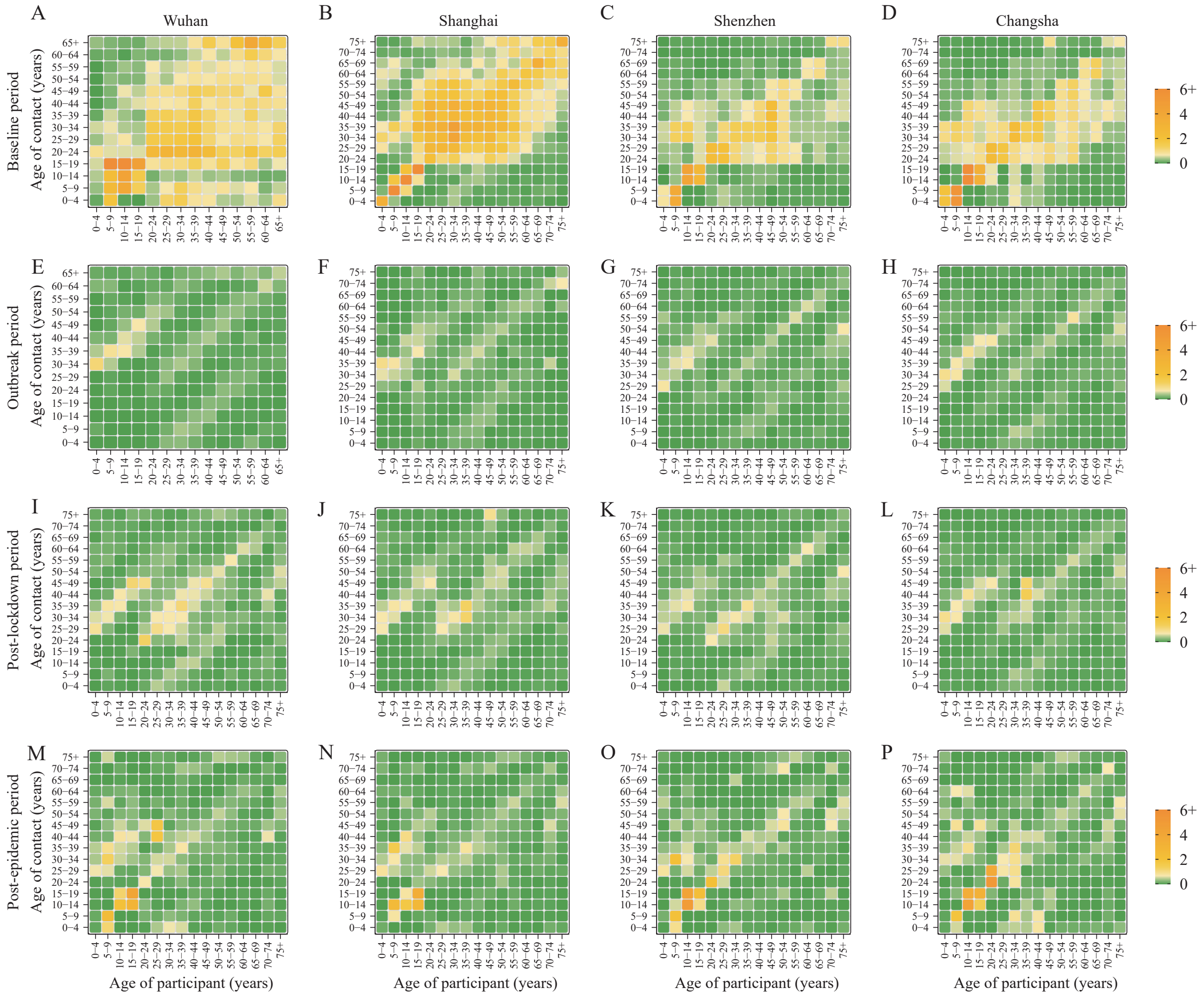

FIGURE 2. Contact matrices by age group for the four study locations for the baseline period in (A–D), outbreak period (E–H), post-lockdown period (I–L), and post-epidemic period (M–P). Each cell of the matrix represents the mean number of contacts that an individual in a given age group has with other individuals, stratified by age groups. The color intensity represents the number of contacts.

previous studies (*7*) (Figure 2A–2D). During the lockdown, most of the classic age-specific features were absent, as the main contributor to contact patterns was the mixing between household members (Figure 2E–2H). Compared to the outbreak period, more contacts gradually occurred among school-age and working-age individuals during the post-lockdown and post-epidemic periods (Figure 2I–2P). During the post-epidemic period, the proportion of household contacts was still remarkably high compared to the pre-COVID era (Figure 2), with household contacts representing approximately half of the total number of recorded contacts (i.e., 48.7% in Wuhan, 53.6% in Shanghai, 43.2% in Shenzhen, and 47.6% in Changsha); the proportion of community contacts was still lower than 20% in the four study locations (i.e., 7.7% in Wuhan, 10.7% in Shanghai, 18.9% in Shenzhen, and 9.5% in Changsha) (Supplementary Table S2, available in https://weekly.chinacdc.cn/).

Assuming a baseline reproduction number of between 1.5 and 3.5 for SARS-CoV-2 considering pre-COVID contact patterns, we used the next-generation matrix approach to investigate the risk of a new epidemic outbreak under the estimated contact patterns during different epidemic phases. Our results show that in the post-epidemic phase, contacts had increased to an extent that would have allowed the emergence of new epidemic outbreaks in fully susceptible populations (as was the case in China at the time of the last survey — November 2020) for R_0 values around 2.5 in Wuhan, Shenzhen, and Changsha, while the risk of resurgence would have been low in Shanghai (Figure 3).

To estimate the effect of social distancing on a possible outbreak of SARS-CoV-2 Omicron BA.5 or another highly transmissible variant, we considered the Shanghai population and assumed an effective reproduction number of 4 [about 20% larger than what was estimated at the onset of the 2022 Omicron BA.2 outbreak in Shanghai (*8*)]. Compared with the baseline scenario considering baseline (pre-COVID) contact patterns, we found that a combination of school closures with a 75% reduction of contacts at the workplace could reduce the infection attack rate by

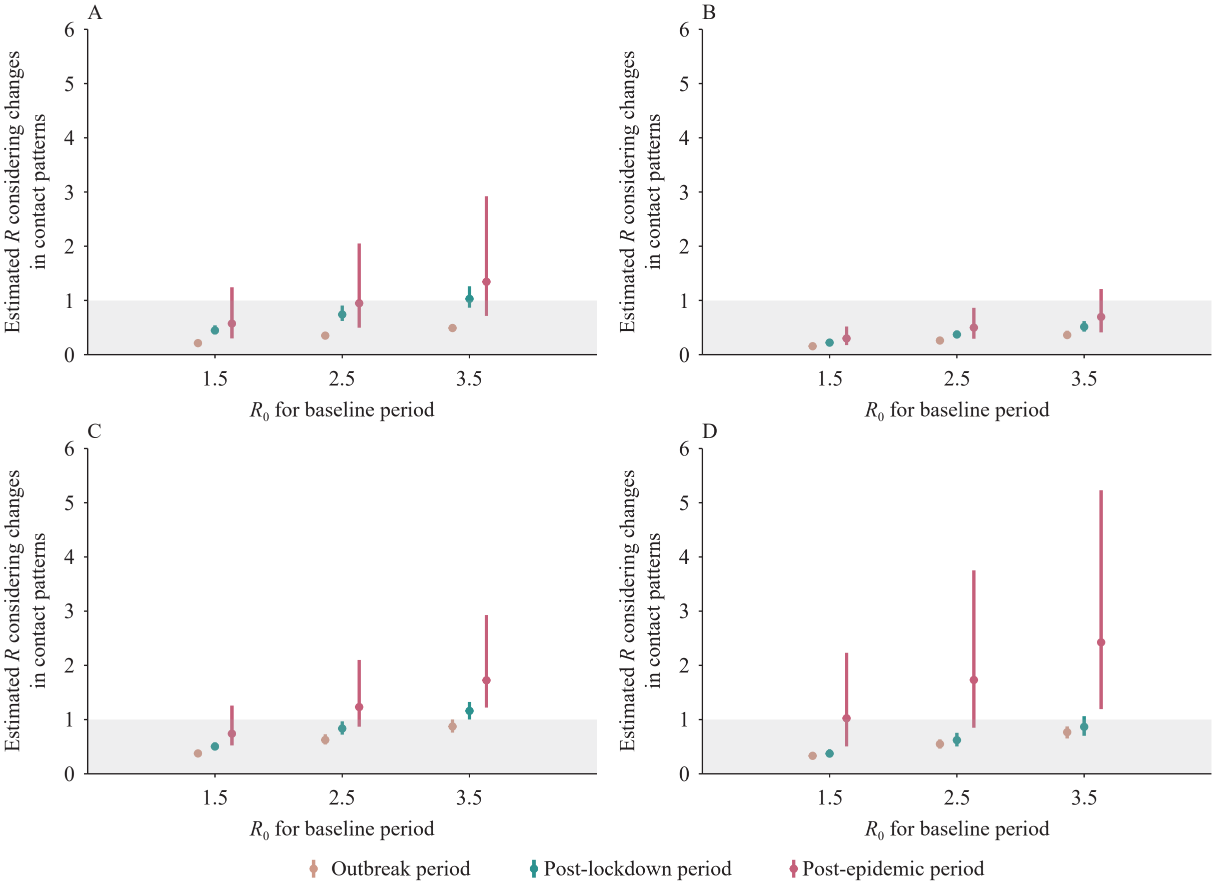

FIGURE 3. Changes in the reproduction number (mean and 95% confidence interval) considering the estimated contact patterns in the different periods in Wuhan (A), Shanghai (B), Shenzhen (C), and Changsha (D).

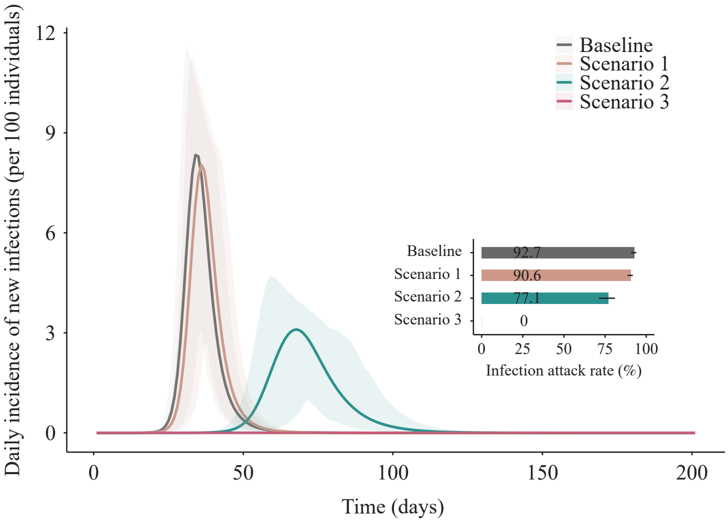

FIGURE 4. The effect of social distancing on the spread of SARS-CoV-2 in Shanghai was examined, assuming an effective reproduction number of 4 and considering baseline (pre-COVID) contact patterns.

Note: The curves show the daily incidence of new infections per 100 individuals (mean and 95% confidence interval) under different social distancing policies. The inset curve shows the infection attack rate (mean and 95% confidence interval) 200 days after the first COVID-19 case. Baseline scenario (no interventions): workplace, school, and community contacts are back to the pre-COVID era; Scenario 1: no contacts at school, while all other contacts are back to the pre-COVID era; Scenario 2: no contacts at school and 75% reduction of contacts at the workplace, while all other contacts are back to the pre-COVID era; Scenario 3: no contacts at school, 75% reduction of contacts at the workplace, and 90% reduction of contacts in the community.

16.8%; an additional 90% reduction of contacts in the community was estimated to be sufficient to control an outbreak (Figure 4).

DISCUSSION

In this study, we quantitatively estimated how human contact patterns by age changed in four Chinese cities during the first year of the COVID-19 pandemic. We found that, although the number of contacts increased in the post-epidemic period (approximately six months after the end of the first COVID-19 wave), the average number of contacts per day remained far from the baseline (pre-COVID) level. In addition to the marked reduction in the mean number of contacts per day, the age of the contacted individuals had markedly changed, highlighting a drop in social interactions with work colleagues and in the community. However, we estimated that the increase in mixing patterns was not sufficient to sustain local transmission in Shanghai, while the risk of an epidemic recurrence in the other three cities remained moderate as of November 2020. During the period of our post-epidemic survey (September 16 to November 8, 2020), fewer than 100 local cases were reported in Chinese mainland, and no local cases were reported in the four study locations, which is consistent with our estimates of the potential reproduction number. Finally, we performed a modeling analysis to evaluate the impact of social distancing in the event of a new SARS-CoV-2 outbreak of Omicron BA.5 or another highly transmissible variant. Our findings support that, although vaccination campaigns conducted in China with current vaccine products (as of 2022) are key to mitigating COVID-19 burden, if policymakers aim to prevent SARS-CoV-2 transmission altogether, social distancing measures are still essential.

Although workplaces, schools, and other public places gradually reopened from February to November 2020, many restrictions were still in place to prevent the resurgence of COVID-19. For example, 1) masks were mandated and body temperature was measured to enter indoor public places (*9*–*10*); 2) indoor mass gatherings were limited in schools (*11*); and 3) cinemas and theaters were operating at 75% or lower capacity, with the audience required to wear face masks and maintain a distance of at least one meter (*12*). From April to August 2020, China experienced several small-scale local outbreaks (*13*). The interventions adopted as well as the fear of infection may explain the slow resumption of contacts highlighted by our surveys in 2020.

Our results are comparable to those obtained in other studies that have assessed changes in contact patterns linked to the relaxation of COVID-19 control measures (*2*,*14*–*17*). After lifting stay-at-home orders and reopening workplaces in China, the United States, and several European countries, the mean number of contacts varied from two to nine per day, which is consistently higher than the number of contacts during lockdowns but significantly lower than the pre-pandemic level. Moreover, similar to Jarvis et al. (*14*), we found a larger proportion of indoor contacts than what was observed in the pre-COVID era.

Our study suffers from the traditional limitations of self-reported contact surveys, including recall, self-reporting, and selection biases, which may have affected our results. Although we explained the anonymity and confidentiality of the survey to study participants, we cannot rule out that the number of contacts may have been underreported during the post-epidemic period, when social distancing and other precautions were still in place. Our modeling analysis is intended to provide only general insights and is based on a set of approximations. For instance, the model does not explicitly consider symptomatic and asymptomatic individuals, pre-symptomatic transmission, the effect of individual-level interventions (e.g., test-trace-isolate, mask wearing), or the level of immunity provided by the primary vaccination cycle. Instead, we combine the effects of all these aspects into a single indicator: the effective reproduction number. Although this allowed us to provide a first-level approximation of the reduction of social contacts, more refined analyses are needed to identify the proper interventions required to contain a novel SARS-CoV-2 outbreak and/or mitigate the COVID-19 burden and pressure on the healthcare system.

Our study quantified contact patterns at different time points during the first year of the COVID-19 pandemic in Chinese mainland and provided evidence of a gradual recovery of contact patterns while social distancing measures were gradually relaxed. Moving forward, monitoring mixing patterns could inform authorities about the risk of resurgence of novel outbreaks caused by highly transmissible SARS-CoV-2 variants, and, in the event of an outbreak, social distancing is likely to play a key role in limiting SARS-CoV-2 transmission and mitigating the burden of COVID-19.

Acknowledgements: Allisandra G. Kummer from Indiana University.

Funding: This work was supported by the Key Program of the National Natural Science Foundation of China (82130093 to H.Y.), Shanghai Municipal Science and Technology Major Project (ZD2021CY001 to H.Y.), and Shanghai Rising-Star Program (22QA1402300 to J.Z.).

doi: 10.46234/ccdcw2023.021

Corresponding authors: Juanjuan Zhang, zhangjuan@fudan.edu.cn; Hongjie Yu, yhj@fudan.edu.cn.

---

[1] School of Public Health, Fudan University, Key Laboratory of Public Health Safety, Ministry of Education, Shanghai Municipality, China; [2] Laboratory for Computational Epidemiology and Public Health, Department of Epidemiology and Biostatistics, Indiana University School of Public Health, Bloomington, IN, USA; [3] Shanghai Institute of Infectious Disease and Biosecurity, Fudan University, Shanghai Municipality, China.

Submitted: November 01, 2022; Accepted: January 19, 2023

REFERENCES

1. Zhang JJ, Litvinova M, Liang YX, Wang Y, Wang W, Zhao SL, et al. Changes in contact patterns shape the dynamics of the COVID-19 outbreak in China. Science 2020;368(6498):1481 – 6. http://dx.doi.org/10.1126/science.abb8001.
2. Zhang JJ, Litvinova M, Liang YX, Zheng W, Shi HL, Vespignani A, et al. The impact of relaxing interventions on human contact patterns and SARS-CoV-2 transmission in China. Sci Adv 2021;7(19):eabe2584. http://dx.doi.org/10.1126/sciadv.abe2584.
3. Zhao YN, O'Dell S, Yang XH, Liao JY, Yang KX, Fumanelli L, et al. Quantifying human mixing patterns in Chinese provinces outside Hubei after the 2020 lockdown was lifted. BMC Infect Dis 2022;22(1):483. http://dx.doi.org/10.1186/s12879-022-07455-7.
4. China Education Daily. News report on the first day of school. 2020. http://www.moe.gov.cn/jyb_xwfb/s5147/202009/t20200902_484234.html. [2021-6-14]. (In Chinese).
5. Leading Group of the People's Republic of China for Response to COVID-19. Instruction on promoting the resumption of work and production. 2020. http://www.gov.cn/zhengce/content/2020-04/09/content_5500698.htm. [2021-6-14]. (In Chinese).
6. Zhang JJ, Klepac P, Read JM, Rosello A, Wang XL, Lai SJ, et al. Patterns of human social contact and contact with animals in Shanghai, China. Sci Rep 2019;9(1):15141. http://dx.doi.org/10.1038/s41598-019-51609-8.
7. Mossong J, Hens N, Jit M, Beutels P, Auranen K, Mikolajczyk R, et al. Social contacts and mixing patterns relevant to the spread of infectious diseases. PLoS Med 2008;5(3):e74. http://dx.doi.org/10.1371/journal.pmed.0050074.
8. Cai J, Deng XW, Yang J, Sun KY, Liu HC, Chen ZY, et al. Modeling transmission of SARS-CoV-2 Omicron in China. Nat Med 2022;28(7):1468 – 75. http://dx.doi.org/10.1038/s41591-022-01855-7.
9. Leading Group of the People's Republic of China for Response to COVID-19. Guidelines for prevention and control of COVID-19 in key places and key populations. 2020.http://www.nhc.gov.cn/xcs/zhengcwj/202004/b90add4a70d042308b8c3d4276ec76a7.shtml. [2021-6-14]. (In Chinese).
10. Ministry of Transport of the People's Republic of China. Regulations for prevention and control of COVID-19 in public transport. 2020. https://mp.weixin.qq.com/s/FivTu0Dw6y_kqIbx8nYKhA. [2021-6-14]. (In Chinese).
11. General Office of the National Health Commission. Guidelines for the prevention and control of COVID-19 in schools during the fall and winter semester 2020. 2020. http://www.nhc.gov.cn/xcs/zhengcwj/202008/c87c05a95153454394b4362dda305340.shtml. [2021-6-14]. (In Chinese).

12. The Ministry of Culture and Tourism of the People's Republic of China. Guidelines for the prevention and control of COVID-19 in performing venues (4th edition). 2020. http://www.gov.cn/xinwen/2020-09/19/content_5544729.htm. [2021-6-14]. (In Chinese).
13. National Health Commission of the People's Republic of China. Daily reports on COVID-19 surveillance in China. http://www.nhc.gov.cn/xcs/yqtb/list_gzbd.shtml. [2021-6-14]. (In Chinese).
14. Jarvis CI, Gimma A, et al. CoMix study - Social contact survey in the UK. 2020. https://cmmid.github.io/topics/covid19/comix-reports.html. [2021-6-14].
15. Coletti P, Wambua J, Gimma A, Willem L, Vercruysse S, Vanhoutte B, et al. CoMix: comparing mixing patterns in the Belgian population during and after lockdown. Sci Rep 2020;10(1):21885. http://dx.doi.org/10.1038/s41598-020-78540-7.
16. Backer JA, Mollema L, Vos ERA, Klinkenberg D, van der Klis FRM, de Melker HE, et al. Impact of physical distancing measures against COVID-19 on contacts and mixing patterns: repeated cross-sectional surveys, the Netherlands, 2016-17, April 2020 and June 2020. Euro Surveill 2021;26(8):2000994. http://dx.doi.org/10.2807/1560-7917.Es.2021.26.8.2000994.
17. Feehan DM, Mahmud AS. Quantifying population contact patterns in the United States during the COVID-19 pandemic. Nat Commun 2021;12(1):893. http://dx.doi.org/10.1038/s41467-021-20990-2.

SUPPLEMENTARY MATERIAL

Inclusion Criteria

Individuals were eligible to participate if they met the following criteria: 1) being a local resident of Wuhan, Shanghai, Shenzhen, or Changsha; 2) having lived in the selected city for more than 6 months in the past year; and 3) being present in the selected city at the time of the interview.

Survey Sampling

We planned to recruit 800 participants for each city, with equal sampling by age groups (0–9 years, 10–19 years, 20–29 years, 30–39 years, 40–49 years, 50–59 years, 60–69 years, 70 years and above) and sex. The survey was conducted through computer-assisted telephone interviews based on a well-established platform (*1*–*3*), which used a computerized random digital dialing system to randomly generate mobile phone numbers from the selected cities and automatically dial to connect with the users. Calls were placed three times on the same day before being classified as invalid. All calls were recorded and spot-checked for quality control of data collection. The person who completed the questionnaire depended on the participant's age and accessibility to mobile phone users, as follows: 1) self-completion and informed consent for participants aged 19–69 years; and 2) guardian-proxy completion for individuals aged 0–18 years or 70 years and above. Participants aged 18 years and below or 70 years and above, especially those without a telephone, were recruited through adults aged 19–69 years living in the same household. Specifically, after a participant aged 19–69 years old finished his/her own questionnaire, the interviewer asked whether there was a household member under 18 or over 70 years old in their household, and the participant could complete a questionnaire on his/her behalf or not. When the phone call was answered, well-trained staff asked participants to complete a questionnaire describing his/her contact behavior. Briefly, participants were asked to record their contact behavior on two different days: the most recent weekday and weekend day.

Data Processing

We recruited participants with roughly equal sample sizes in eight age groups (0–9 years, 10–19 years, ..., 60–69 years, 70 years and above) and by sex. To obtain a representative sample of the general population, we resampled the original data using multiple-stage bootstrapping, adjusting for age, sex, household size, day type (i.e., weekdays and weekends), and the probability of being a student or worker by age group.

Modeling SARS-CoV-2 Transmission Estimation of the Reproduction Number

The reproduction number, R, was estimated using a next-generation matrix approach based on the age-specific contact matrix for the COVID-19 outbreak period, the post-lockdown period, and the post-epidemic period, as estimated from our survey in Wuhan, Shanghai, Shenzhen, and Changsha, according to the following equation:

$$R_0 = \frac{\beta}{\gamma}\rho(M)$$

Where,

β is the transmission rate;

γ is the recovery rate. In an SIR model, the recovery rate is equivalent to the inverse of the duration of the generation time.

$\rho(M)$ is the spectral radius of matrix M and whose element Mij represents the average number of contacts between individuals in age group i with individuals in age group j.

Impact of Social Distancing and Vaccination Strategies on the SARS-CoV-2 Transmission

To estimate the impact of social distancing and vaccination strategies on the transmission dynamics of SARS-CoV-2, we implemented a classic age-structured Susceptible-Infectious-Removed (SIR) model for the Shanghai population. Briefly, susceptible and partially protected individuals (i.e., individuals who were previously infected or

SUPPLEMENTARY TABLE S1. Mean number and 95% *CI* of reported contacts by respondent characteristics and locations in the baseline, outbreak and post-epidemic periods.

Characteristics	Wuhan, mean (95% *CI*)			Shanghai, mean (95% *CI*)			Shenzhen, mean (95% *CI*)			Changsha, mean (95% *CI*)		
	Baseline†	**Outbreak†**	**Post-epidemic§**	**Baseline†**	**Outbreak†**	**Post-epidemic§**	**Baseline†**	**Outbreak†**	**Post-epidemic§**	**Baseline†**	**Outbreak†**	**Post-epidemic§**
Overall	14.6 (13.3, 16.1)	2 (1.9, 2.1)	3.9 (3, 5.3)***	18.9 (17.7, 20.1)	2.3 (2.0, 2.8)	2.8 (2.4, 3.1)***	7.9 (7.3, 8.7)	2.2 (2.1, 2.3)	3.7 (2.8, 4.6)***	9.5 (8.7, 10.4)	2.2 (2.0, 2.3)	4.2 (3.3, 5.3)***
Sex												
Female	14.7 (12.9, 16.5)	2.1 (2.0, 2.3)	4.1 (2.8, 6.0)***	18.6 (16.9, 20.2)	2.6 (2.1, 3.4)	2.4 (2.1, 2.8)***	7.2 (6.5, 8.2)	2.1 (2.0, 2.2)	3 (2.3, 3.8)***	9.3 (8, 10.7)	2.1 (1.9, 2.2)	4.7 (3.4, 6.3)***
Male	14.5 (12.2, 17.1)	1.8 (1.7, 2.0)	3.8 (2.6, 6.1)***	19.2 (17.6, 20.5)	2.1 (1.9, 2.4)	3.2 (2.6, 3.9)***	8.6 (7.8, 9.5)	2.2 (2.0, 2.4)	4.3 (3.1, 6)***	9.8 (8.8, 10.9)	2.3 (2.1, 2.5)	3.8 (3.1, 4.6)***
Age group (years)												
0–6	8.4 (2.8, 18.5)	2.2 (1.7, 2.7)	3.3 (2.3, 4.3)***	11.5 (9.4, 14)	1.9 (1.6, 2.2)	2.7 (2.2, 3.5)***	7 (4.9, 9.5)	2.6 (2.3, 2.9)	3.1 (2.5, 3.8)***	11.1 (8.3, 14)	2.7 (2.3, 3.0)	3.4 (2.7, 4.1)***
7–19	16.1 (13.4, 20.2)	2.1 (2.0, 2.2)	9 (4.8, 16.1)***	26.9 (23.7, 30.3)	2.6 (2.0, 3.5)	7.9 (4.7, 11.7)***	11.6 (9.9, 14.1)	2.5 (2.2, 2.8)	7.2 (3.8, 11.4)***	16.6 (13.9, 19.6)	2.2 (2.1, 2.4)	8.7 (5.9, 12.2)***
20–39	15.2 (13.1, 17.7)	2.1 (1.9, 2.3)	4.7 (2.8, 7.5)***	22.4 (19.4, 25.7)	2.2 (2.0, 2.5)	2.5 (2.2, 2.8)***	8.0 (7.2, 9.0)	1.8 (1.6, 1.9)	3.4 (2.4, 4.7)***	9.0 (7.6, 11.1)	2.2 (1.9, 2.5)	4.9 (3.1, 7.6)***
40–59	13.8 (10.8, 16.3)	2.0 (1.9, 2.1)	2.3 (2.0, 2.7)***	19.9 (17.1, 22.8)	2.9 (2.0, 4.1)	2.5 (2.0, 3.1)***	8.5 (6.9, 10)	2 (1.8, 2.3)	2.6 (2.1, 3.1)***	9.3 (7.8, 11.3)	2.1 (1.9, 2.3)	2.9 (2, 4.7)***
≥60	14.0 (8.1, 20.2)	1.4 (1.2, 1.7)	1.7 (1.4, 1.9)***	12.7 (10.9, 14.3)	1.5 (1.3, 1.8)	1.7 (1.4, 2)***	5 (4.4, 5.7)	2.3 (2.1, 2.5)	2.2 (1.7, 2.9)**	5.4 (4.6, 6.2)	2.0 (1.8, 2.2)	2.3 (1.9, 2.7)***
Type of profession												
Pre-school	8.4 (2.8, 18.5)	2.2 (1.7, 2.7)	2.6 (2.2, 3.3)***	10.5 (8.3, 13)	1.9 (1.6, 2.2)	2.7 (2.2, 3.5)	5.0 (3.1, 7.5)	2.6 (2.2, 2.9)	3.1 (2.5, 3.8)***	8.6 (6, 11.9)	2.7 (2.3, 3.2)	3.0 (2.5, 3.6)***
Students	14.7 (11.8, 18.2)	2.1 (2.0, 2.3)	8.9 (5.1, 15.3)***	26.1 (23.2, 29.1)	2.5 (2.1, 3.3)	8.7 (5.2, 13.2)***	11.9 (10.4, 13.8)	2.6 (2.3, 2.8)	7.7 (4.6, 11.6)***	16.7 (14.5, 19)	2.3 (2.2, 2.5)	9.6 (6.1, 14.3)***
Employed	15.3 (13.6, 16.9)	2.1 (1.9, 2.2)	4.0 (2.7, 6.0)***	22.4 (20.6, 24.3)	2.6 (2.1, 3.2)	2.7 (2.4, 3.2)***	9.3 (8.5, 10.2)	2.0 (1.8, 2.2)	3.2 (2.4, 4.4)***	10.3 (8.9, 11.7)	2.2 (2.0, 2.4)	3.8 (2.8, 5.3)***
Working-age not in the labor force	13.9 (6.0, 21.6)	1.8 (1.4, 2.4)	2.2 (1.9, 2.6)***	15.4 (7.4, 24.5)	1.8 (1.3, 2.3)	2.0 (1.6, 2.4)***	5.8 (3.6, 9.4)	1.7 (1.4, 2.1)	2.1 (1.8, 2.6)***	5.5 (4.1, 7.4)	2.1 (1.8, 2.4)	2.5 (2, 3.2)***
Retired	12.3 (8, 18.6)	1.5 (1.4, 1.8)	1.8 (1.6, 2)***	11.8 (10.4, 13.4)	1.6 (1.3, 1.8)	1.7 (1.5, 1.9)***	4.8 (4.1, 5.4)	2.2 (2.0, 2.3)	2.1 (1.6, 2.7)*	5.1 (4.4, 5.8)	1.9 (1.7, 2.1)	2.1 (1.8, 2.4)***
Household size												
1	10.8 (5.7, 18.2)	0.6 (0.1, 1.5)	1.0 (0.5, 1.9)***	15.2 (10.5, 21.1)	0.3 (0.2, 0.5)	1.0 (0.8, 1.5)***	5.5 (4.2, 6.9)	0.8 (0.6, 1.0)	2.3 (1.1, 4.2)***	5.6 (4.0, 7.6)	0.9 (0.4, 1.7)	1 (0.5, 1.9)
2	12.5 (7.4, 16.3)	1.1 (0.9, 1.3)	2.7 (1.4, 6.5)***	14.6 (12.8, 16.9)	1.4 (1.1, 1.8)	2.1 (1.6, 2.8)***	6.4 (4.9, 8.0)	1.3 (1.1, 1.4)	3.3 (1.5, 7.1)***	6.4 (5.4, 7.7)	1.4 (1.2, 1.6)	2.7 (1.7, 4.4)***
3	14.7 (13, 16.5)	1.9 (1.8, 2.0)	3.9 (2.9, 6.1)***	20.3 (18.6, 21.9)	2.2 (2.0, 2.3)	3.4 (2.7, 4.4)***	8.8 (8.0, 9.8)	2.3 (2.2, 2.5)	4.8 (3.2, 6.7)***	11.4 (9.8, 13.0)	2.2 (2.1, 2.3)	4.1 (2.8, 5.9)***
4	11.9 (9.1, 15.3)	2.3 (2.2, 2.5)	3.7 (3.3, 4.2)***	20.2 (16.9, 23.7)	3.0 (2.8, 3.2)	4.9 (3.3, 7.7)***	8.3 (7.3, 9.4)	3.1 (2.9, 3.2)	4.3 (3.5, 5.4)***	10.9 (8.5, 13.4)	3.0 (2.8, 3.1)	6.6 (4.4, 10.1)***
≥5	21.7 (16.9, 25.5)	3.2 (2.8, 3.4)	11.0 (5.3, 20.6)***	21.5 (18.1, 24.2)	6.0 (3.9, 8.9)	5.6 (4.8, 6.5)	10.1 (8.3, 12.4)	4.3 (4.1, 4.5)	4.5 (2.7, 6.1)**	11.3 (8.8, 14.2)	3.9 (3.7, 4.1)	6.0 (4.1, 8.2)***

TABLE S1. (Continued)

Characteristics	Wuhan, mean (95% *CI*)			Shanghai, mean (95% *CI*)			Shenzhen, mean (95% *CI*)			Changsha, mean (95% *CI*)		
	Baseline[†]	**Outbreak[†]**	**Post-epidemic[§]**	**Baseline[†]**	**Outbreak[†]**	**Post-epidemic[§]**	**Baseline[†]**	**Outbreak[†]**	**Post-epidemic[§]**	**Baseline[†]**	**Outbreak[†]**	**Post-epidemic[§]**
Day type[¶]												
Weekday	14.6 (13.3, 16.1)	–	4.5 (3.3, 6.0)	20.3 (18.9, 21.8)	–	3.2 (2.7, 3.6)	7.9 (7.3, 8.7)	–	4.2 (3.2, 5.5)	9.5 (8.7, 10.4)	–	4.9 (3.8, 6.2)
Weekend	–	–	2.7 (2.0, 5.4)	14.6 (12.8, 16.7)	–	1.8 (1.6, 2.1)	–	–	2.4 (1.5, 4.0)	–	–	2.6 (2.0, 3.6)

* $P<0.05$, ** $P<0.01$, *** $P<0.001$. *P*-values are taken from a bootstrap one sample *t* test distinguishing the post-epidemic period from the outbreak period.

[†] The 95% confidence interval (*CI*) on mean for baseline and outbreak periods were calculated by bootstrap sampling. Specifically, the 95% *CI* are 2.5% quantiles and 97.5% quantiles of 100 means calculated from 100 representative samples.

[§] The mean of contacts and 95% confidence interval on mean for post-epidemic period are calculated based on bootstrap-adjusted samples. Specifically, the 95% *CI* are 2.5% quantiles and 97.5% quantiles of 100 means calculated from 100 representative samples.

[¶] For students and workers, the weekday refers to the day going to work/school. For baseline period of Wuhan, Shenzhen, and Changsha, we only investigated the contact patterns of weekdays. For outbreak period, weekdays and weekends are not distinguished due to the lockdown.

SUPPLEMENTARY TABLE S2. Mean of the number of reported contacts by setting during post-epidemic period.

City	Overall, mean (95% *CI*)*	Household, mean (%)*,†	Workplace, mean (%)*,†	School, mean (%)*,†	Community, mean (%)*,†
Wuhan	3.9 (3.0, 5.3)	1.9 (48.7)	0.9 (23.1)	1.0 (25.6)	0.3 (7.7)
Shanghai	2.8 (2.4, 3.1)	1.5 (53.6)	0.6 (21.4)	0.5 (17.9)	0.3 (10.7)
Shenzhen	3.7 (2.8, 4.6)	1.6 (43.2)	0.9 (24.3)	0.9 (24.3)	0.7 (18.9)
Changsha	4.2 (3.3, 5.3)	2.0 (47.6)	0.9 (21.4)	1.3 (31.0)	0.4 (9.5)

* The mean and 95% confidence interval (*CI*) of mean were calculated based on bootstrap-adjusted samples. Specifically, the 95% *CI* are 2.5% quantiles and 97.5% quantiles of 100 means calculated from 100 representative samples.

† Proportion of the overall number of reported contacts were calculated as dividing the mean of each setting by the mean of overall contacts. As some contacts occurred at multiple locations, the sum of proportion may exceed 100%.

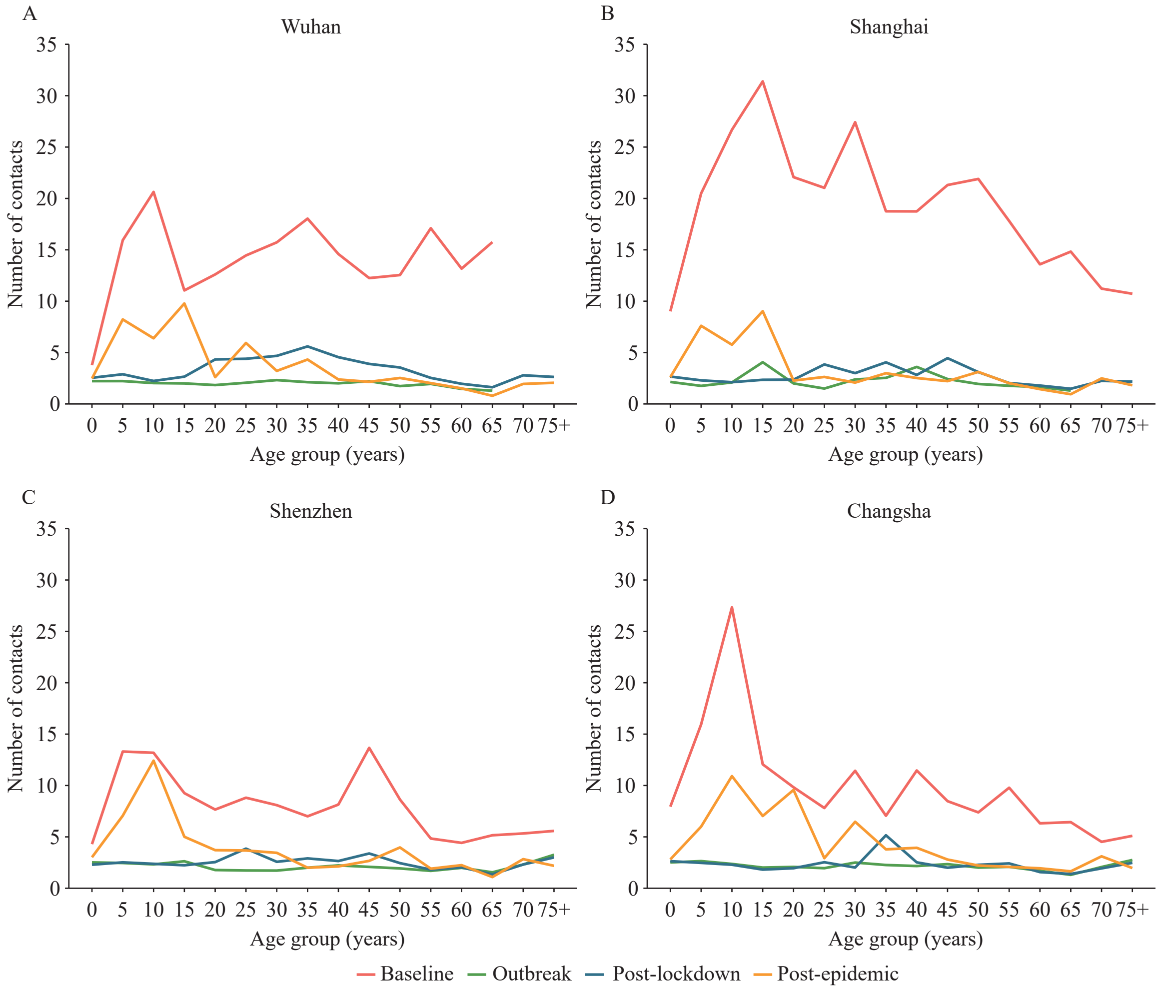

SUPPLEMENTARY FIGURE S1. Mean number of reported contacts by participant age during the baseline, outbreak, post-lockdown, and post-epidemic periods in (A) Wuhan, (B) Shanghai, (C) Shenzhen, and (D) Changsha.
Note: The last age group for the baseline and outbreak periods in Wuhan, and the outbreak period in Shanghai, was 65 years and older due to the small sample size of older people.

vaccinated but whose immunity to infection has waned) can acquire the infection through contacts with infectious individuals. Infectious individuals move to the removed compartment after an average infectious period of length equivalent to the generation time (*4*). Individuals in the removed compartment (corresponding to temporarily protected individuals) were not involved in the transmission process. Given that we were interested in simulating a short period of time (a few months), we did not consider waning of protection and thus removed individuals could not be re-infected.

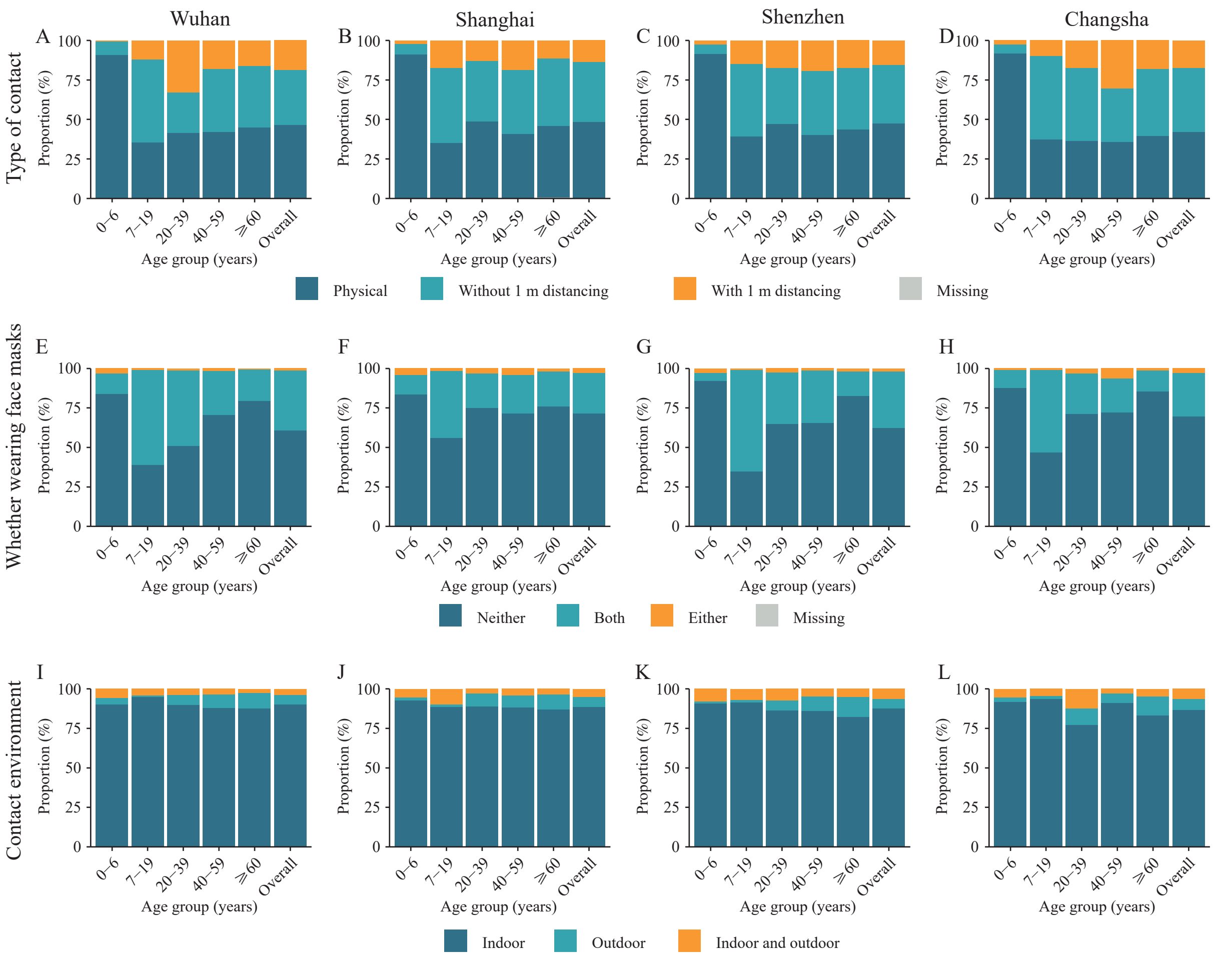

SUPPLEMENTARY FIGURE S2. Contact type, contacts with face masks, and contact environment by age. (A) The proportion of physical contacts, non-physical contacts without 1m distancing, and non-physical contacts with 1m distancing by age for Wuhan. (B–D) The same proportions for Shanghai, Shenzhen, and Changsha, respectively. (E–H) The same proportions as (A–D), but for whether the participants and contacts were wearing face masks. (I–L) The same proportions as (A–D), but for the proportion of contacts that occurred indoors, outdoors, and both.

Each model compartment is divided into sixteen 5-year age groups (0–4, 5–9, …, 60–64, 75 years and above). Susceptible and partially protected individuals are exposed to an age-specific force of infection regulated by the average number of contacts per day that individuals of a given age group have with individuals of all age groups (i.e., the contact matrix). We used the following set of differential equations to simulate this process:

$$\begin{cases} \dot{S}_i = -\beta \sum_{j=1}^{n} M_{ij} \dfrac{I_j}{N_j} S_i \\ \dot{I}_i = \beta \sum_{j=1}^{n} M_{ij} \dfrac{I_j}{N_j} S_i - \gamma I_j \\ \dot{R}_i = \gamma I_j \end{cases}$$

where,

i and *j* represent the age group;

n=16 is the total number of age classes;

Si is the number of susceptible/partially protected individuals in age group *i*;

Ii is the number of infectious individuals in age group *i*;

Ri is the number of recovered/temporarily protected individuals in age group *i*;

Ni is the total number of individuals in age class *i* (i.e., *Ni*= *Si* + *Ii* + *Ri*). The age structure was derived from Shanghai official records and the total population size is 24,197,001 (*5*).

β is the transmission rate, which is determined to obtain the desired value of the reproduction number using the next generation matrix approach;

γ is the recovery rate. In an SIR model, the recovery rate is equivalent to the inverse of the duration of the generation time, which was estimated to be 5.1 days (*6*).

Mij is the average number of contacts between individuals in age group *i* with individuals in age group *j*.

REFERENCES

1. Zhang JJ, Litvinova M, Liang YX, Wang Y, Wang W, Zhao SL, et al. Changes in contact patterns shape the dynamics of the COVID-19 outbreak in China. Science 2020;368(6498):1481 – 6. http://dx.doi.org/10.1126/science.abb8001.
2. Zhang JJ, Litvinova M, Liang YX, Zheng W, Shi HL, Vespignani A, et al. The impact of relaxing interventions on human contact patterns and SARS-CoV-2 transmission in China. Sci Adv 2021;7(19):eabe2584. http://dx.doi.org/10.1126/sciadv.abe2584.
3. Wang LP, Cowling BJ, Wu P, Yu JX, Li F, Zeng LJ, et al. Human exposure to live poultry and psychological and behavioral responses to influenza A(H7N9), China. Emerg Infect Dis 2014;20(8):1296 – 305. http://dx.doi.org/10.3201/eid2008.131821.
4. Liu QH, Ajelli M, Aleta A, Merler S, Moreno Y, Vespignani A. Measurability of the epidemic reproduction number in data-driven contact networks. Proc Natl Acad Sci USA 2018;115(50):12680 – 5. http://dx.doi.org/10.1073/pnas.1811115115.
5. Shanghai Municipal Bureau of Statistics. Shanghai Statistical Yearbook 2017. 2017. https://tjj.sh.gov.cn/tjnj/20190117/0014-1001529.html. [2020-9-1]. (In Chinese).
6. Zhang JJ, Litvinova M, Wang W, Wang Y, Deng XW, Chen XH, et al. Evolving epidemiology and transmission dynamics of coronavirus disease 2019 outside Hubei province, China: a descriptive and modelling study. Lancet Infect Dis 2020;20(7):793 – 802. http://dx.doi.org/10.1016/s1473-3099(20)30230-9.

Indexed by Science Citation Index Expanded (SCIE), Social Sciences Citation Index (SSCI), PubMed Central (PMC), Scopus, Chinese Scientific and Technical Papers and Citations, and Chinese Science Citation Database (CSCD)

The inauguration of *China CDC Weekly* is in part supported by Project for Enhancing International Impact of China STM Journals Category D (PIIJ2-D-04-(2018)) of China Association for Science and Technology (CAST).

CCDC weekly

Vol. 5 No. 5 Feb. 3, 2023

Responsible Authority
National Health Commission of the People's Republic of China

Sponsor
Chinese Center for Disease Control and Prevention

Editing and Publishing
China CDC Weekly Editorial Office
No.155 Changbai Road, Changping District, Beijing, China
Tel: 86-10-63150501, 63150701
Email: weekly@chinacdc.cn

CSSN
ISSN 2096-7071
CN 10-1629/R1